

The Io Neutral Clouds and Plasma Torus

N. Thomas

Physikalisches Institut, University of Berne

F. Bagenal

LASP and Dept. of Astrophysical & Planetary Sciences, University of Colorado

T. W. Hill

Dept. of Physics & Astronomy, Rice University

J. K. Wilson

Center for Space Physics, Boston University

23.1 OVERVIEW

The interaction between Io's atmosphere and Jupiter's magnetosphere results in a significant mass loss from Io. Some of the material lost is directly picked up from Io's exosphere in the form of ions. A significant fraction, however, escapes as neutral atoms and molecules, principally oxygen and sulfur atoms and their compounds (see Section 23.2). These neutrals accompany Io in its orbit about Jupiter (5.91 jovian radii, R_J , from the center of the planet) until they are ionized through electron impact and charge exchange. The relative importance of ionization in Io's near vicinity (less than a few Io radii) with respect to ionization remote from Io (greater than a few Io radii) is an outstanding question. Once ionized, however, the ions are accelerated to the nearly corotational flow of the ambient plasma (see Section 23.3), which passes Io at a relative velocity of $\sim 54 \text{ km s}^{-1}$, to form a torus of ions (the Io plasma torus) completely surrounding Jupiter (Figure 23.1).

The first observational evidence of these processes was the detection of sodium D-line emission (at 589.0 and 589.6 nm) from a "cloud" in the vicinity of Io (Brown 1974). It was quickly established that resonant scattering of sunlight was producing the observed emission (Trafton *et al.* 1974, Brown and Yung 1976). It was also suggested that the neutrals were being removed from Io by charged particle sputtering of its surface and/or atmosphere (Matson *et al.* 1974, Haff *et al.* 1981). Following the *Voyager 1* observations of Io, which revealed an SO_2 atmosphere (Pearl *et al.* 1979) and a sulfur-dominated surface (Sagan 1979), it became widely assumed that Na was merely a trace element in a neutral cloud dominated by sulfur and oxygen atoms and their compounds. Sodium remains by far the most frequently observed species, its emission being 30 times brighter than any other at visible and near infrared wavelengths. These early discoveries and initial modeling were reviewed in Pilcher and Strobel (1982).

Images of the sodium cloud have been acquired since the

early 1980s (e.g., Goldberg *et al.* 1984) and models of the sputtered neutral clouds showed that electron impact ionization and charge exchange with torus plasma were significant loss processes on timescales of a few hours (e.g., Smyth and Combi 1988, Smyth 1992). Hence, the observed distributions of the neutral clouds are dependent upon the spatial distribution of the torus plasma. Imaging studies also began to reveal that sputtering was not the only escape mechanism. This became even more clear when wide-field observations showed that sodium emission extends out to at least $500 R_J$ from the planet (Mendillo *et al.* 1990). To reach these distances, iogenic neutrals must be accelerated to above jovian escape velocity. Models constrained by detailed observations of characteristic structures (Section 23.2.1) have shown the presence of a number of acceleration mechanisms both at Io itself and in the torus (Wilson *et al.* 2002).

Investigations of the ionized material began with measurements by the *Pioneer 10* UV photometer (Carlson and Judge 1975) which suggested a high density of low atomic weight ions in Jupiter's magnetosphere. However, the interpretation was not straightforward and most of the original conclusions have subsequently been proven incorrect. However, Kupo *et al.* (1976) detected emission from the collisional excitation of S^+ (at 671.6 and 673.1 nm) near Io's orbit and the line ratio, which R. Brown (1976) also recognized to be diagnostic of electron density (n_e), indicated $n_e = 1-3 \times 10^3 \text{ cm}^{-3}$. Emission from O^+ (at 372.7 and 372.9 nm) was detected by Pilcher and Morgan (1979) shortly before the *Voyager 1* flyby in March 1979.

The *Voyager 1* plasma science (PLS) and ultraviolet spectrometer (UVS) experiments provided a data set which remained the most detailed measurements of the low energy heavy ion population in Jupiter's magnetosphere for nearly 20 years. From these data, the 2-D spatial distributions of the major ion species (S^+ , S^{2+} , S^{3+} , O^+ , and O^{2+}) and n_e have been derived (Bagenal 1994). The radial dependence of composition is shown in Figure 23.2 and is discussed in

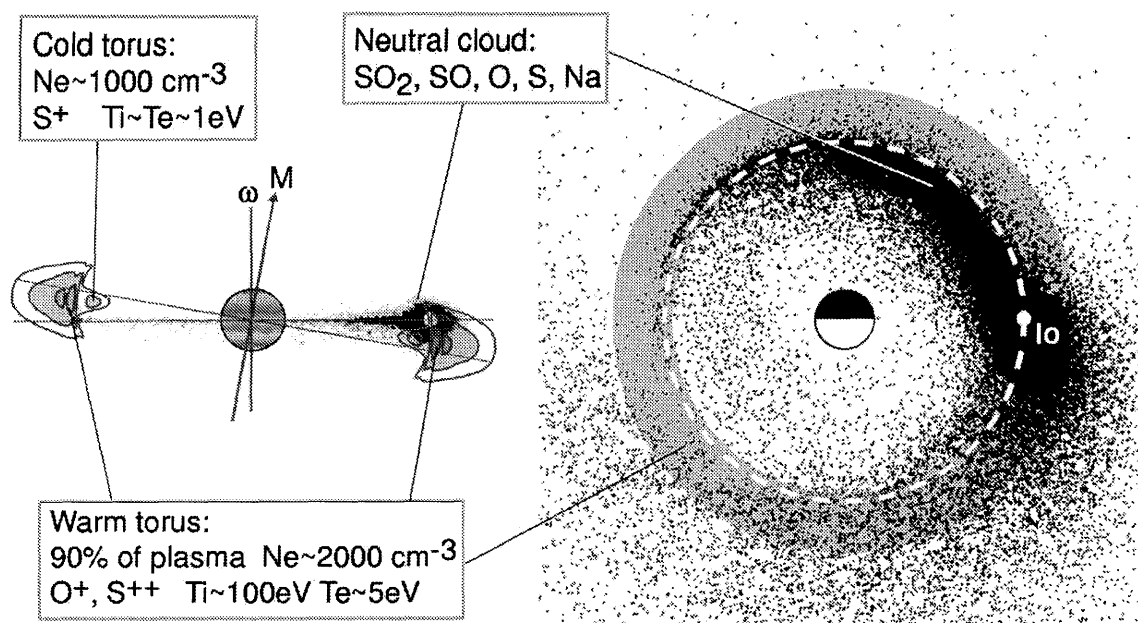


Figure 23.1. Cartoon of the Io neutral clouds and plasma torus. Left: view from central meridian longitude of 290° . Jupiter's magnetic axis (M) is tilted 9.6° from the rotation axis (Ω). The plasma torus is centered on the centrifugal equator which is $\sim 2/3 \times 9.6^\circ$ from the rotational equator and plane of Io's orbit. Right: view looking down over Jupiter's north pole. The shapes of the clouds of neutral species varies between species, the longer-lived species (S , O) being more extended from Io than species that are easily dissociated and/or ionized (SO_2 , Na).

more detail in Section 23.5. The spatial distribution of n_e is also illustrated. This distribution we will refer to as a “benchmark” to compare other observations against. Such an approach has proven necessary because of the highly time variable nature of the system and the need to compare observations from different epochs.

For many purposes, Jupiter's magnetic field configuration near Io's orbit can be assumed to be a dipole which is slightly offset from the center of Jupiter and tilted by 9.6° with respect to the rotation axis towards a System III magnetic longitude (λ_{III}) of 200° (Connerney *et al.* 1998). Only for detailed observations are higher order models (Chapter 24) necessary. Because of this it is often convenient to describe positions in the magnetic field in terms of the equatorial distance of a dipolar magnetic flux tube, L (Roederer 1970). Ions injected at or near Io are picked up and begin to oscillate along field lines about an equilibrium position which is defined for a multi-species plasma by the balance between magnetic mirror force (with possible ion anisotropy), centrifugal force and the ambipolar-electric field. The equilibrium position is close to a plane defined by the points on each magnetic field line which are furthest away from the rotation axis (the centrifugal equator). This is located $2/3$ of the way to the magnetic equator from the rotational equator. The exact position is, however, a weak function of ion temperature (T_i) becoming closer to the magnetic equator as T_i increases (Hill *et al.* 1974, Cummings *et al.* 1980). The ions undergo collisions and become distributed latitudinally along the field lines according to the bulk parallel temperature (T_{\parallel}). It is not known whether the plasma is isotropic, i.e., $T_{\perp} = T_{\parallel} = T_i$ (see Roederer 1970), but it is often assumed to be and the best evidence available (e.g., Woodward 1992, Cray *et al.* 1996) seems to support this although there must be anisotropy at some level

resulting from, for example, the pickup process. The benchmark distribution is then constructed by extrapolating local measurements along the *Voyager 1* trajectory (constrained by UVS measurements) using the above description of the forces on the plasma.

Ground-based measurements have essentially confirmed this basic structure (Trauger 1984). From the benchmark, one can make some estimates of torus bulk properties. For example, the total torus mass can be estimated by assuming a torus volume (typically $1.4 \times 10^{25} \text{ m}^3$ if one assumes a cross-sectional area of $1 R_J^2$) filled with a mean density of $2000 \text{ ions cm}^{-3}$ of a mean molecular weight of 20. This results in a mass of $9.3 \times 10^8 \text{ kg}$. At any given time, the total mass can differ from this value by at least 50% because of the variability of the whole system.

It is widely assumed that the total mass loss from Io is around 1 ton s^{-1} although there are again large uncertainties because of observational constraints on certain, possibly significant, loss processes. A major fraction of the mass removed from Io (probably about $2/3$) is ejected out of the jovian system via charge-exchange processes on short timescales. For the remaining material, the mean residence time for torus ions probably lies between 25 and 80 days. If expansion into the middle magnetosphere were the main loss mechanism, this implies a mean outflow velocity of the order of 50 m s^{-1} .

Processes that are not well understood distribute the plasma radially and lead to a spatial distribution of plasma which is not uniform, either in density or temperature (Section 23.4). Regions within the torus are categorized by their ion temperature. T_i is at a maximum near Io's orbit and decreases rapidly inwards towards Jupiter. T_i probably decreases as one moves outwards towards the middle magnetosphere. However, there remains some inconsistency in the

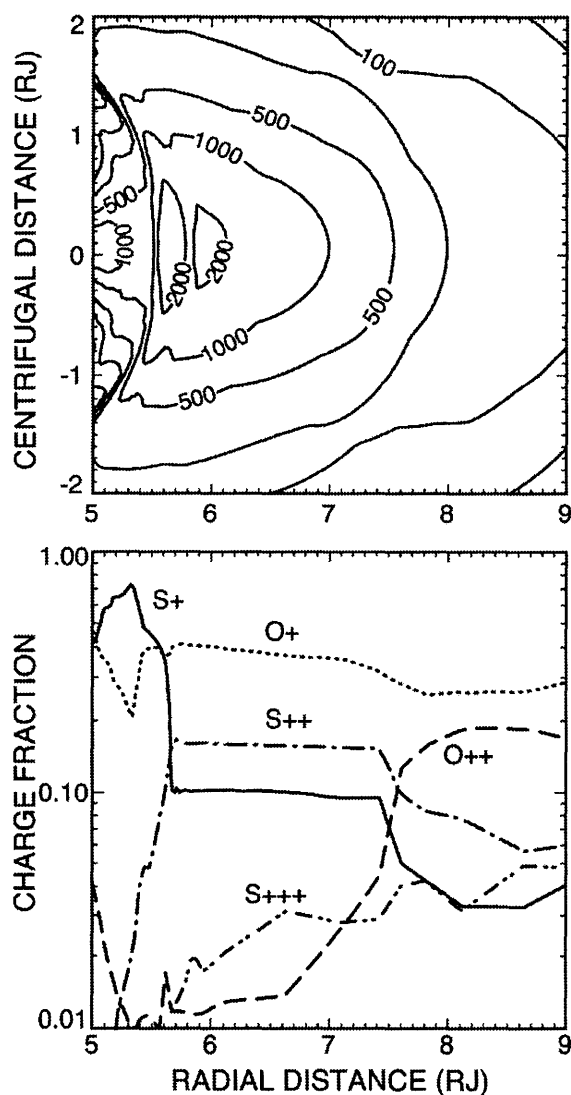


Figure 23.2. Plasma conditions measured by *Voyager 1* near the dusk meridian on March 6, 1979. Top: Contours of electron density (cm^{-3}) as a function of radial distance and distance from the centrifugal equator. Bottom: Ion composition (ion density divided by electron density) derived from emissions measured by *Voyager* UVS $>5.7 R_J$ and from in situ measurements of the *Voyager* PLS instrument $<5.7 R_J$. These results are used as a “benchmark” but many observations indicate that variations in density and composition with time occur. (From Bagenal 1994.)

observations with some results indicating constant or even increasing T_i with distance in this region. This temperature structure is related, in part, to inward transport being much slower than outward transport. At $L = 6$, the ions in the torus are around 100 eV ($1 \text{ eV} = 1.16 \times 10^4 \text{ K}$) but this temperature is variable with space and probably with time. It is, however, always considerably less than the pickup energy of either sulfur (540 eV) or oxygen (270 eV) at Io’s orbit. The drop in T_i inward occurs over a very short distance. At $L = 5$, the plasma is extremely cold ($<2 \text{ eV}$) and is strongly confined to the centrifugal equator. This region is referred to as the cold torus. In principle, from $L = 6$ outwards into the warm outer torus, T_i should decrease with

distance because of the expansion and continuing radiative energy loss.

The spatial distribution of plasma in the torus is complicated by the nature of the source distribution, plasma transport, the sink distribution, and energy transfer. The density variation with distance is dependent upon (1) the distribution of source ions (which is not entirely local to Io and is affected by Io’s motion with respect to the magnetic field), (2) the ion temperature (because the latitudinal expansion along the field line is proportional to $T_i^{1/2}$), (3) the transport process (which is not clearly established but probably strongly dependent upon L), (4) L^3 (because the volume of a flux tube increases with distance from Jupiter), (5) energy transfer processes and (6) the sink processes. It should also be noted that these processes are, to some extent, interdependent. The source affects T_i through the pickup process, for example. There also appear to be external effects, such as the dawn–dusk electric field (Section 23.4.6) which produces a shift in the position of the axis of symmetry. These effects may themselves be related to the sources, transport, and sinks of iogenic material.

Although Io is the source of most material in the torus, the peak density is located inside Io’s orbit in the benchmark case. Ground-based observations of S^+ show an intensity peak which is rather narrow ($\approx 0.1 R_J$) in radial extent and is so prominent in ground-based observations of S^+ that it has been named the “ribbon” (Trauger 1984). It is inferred (although not necessarily true) that the “ribbon” is a tracer for the position of maximum density in the torus. However, the density distributions of the individual species are further complicated by electron temperature (T_e) dependent ionization, recombination, and charge-exchange reactions. T_e does not track T_i . It is around 4.5 eV near Io’s orbit and, like T_i , drops as one moves inward, reaching values of $\leq 1 \text{ eV}$ at $L = 5$. Outside Io’s orbit, T_e clearly rises to 8 eV at $L = 7.5$ (Sittler and Strobel 1987, Frank and Paterson 2000a). This increase in T_e with radial distance results in a change in the ionization state although it is important to note that the system does not reach chemical equilibrium. Mass loss occurs over a shorter timescale than the time needed to reach chemical equilibrium. Thus, while both n_e and the S^+ density are still fairly high inside $5.6 R_J$, S^{2+} is almost negligible at this point because T_e is not high enough to ionize the S^+ . Starting at the position of the ribbon, increasing amounts of S^{2+} , S^{3+} , and O^{2+} are present, with S^{2+} becoming the dominant sulfur species outside Io’s orbit.

In the years immediately following the *Voyager* flyby, the total radiated power from the torus was estimated to be at least $2.5 \times 10^{12} \text{ W}$ (Shemansky 1980). This was based on the extrapolation of UVS data using chemical models and then determination of the total radiative loss via radiative cooling coefficients. At this time, T_e was still estimated to be much higher than now appears to be the case. By 1988, the proposed composition of the torus at the time of the *Voyager 1* encounter had stabilized at a lower T_e and lower ionization state. From revised analysis of the radiated energy, it was concluded that the torus loses around $0.63 \times 10^{-12} \text{ erg cm}^{-3} \text{ s}^{-1}$ (Shemansky 1988) which, when combined with our estimated torus volume, gives $8.8 \times 10^{11} \text{ W}$. Again, this is highly time variable (Section 23.5) and at the time of the *Voyager 2* encounter, the radiated energy was probably well in excess of 10^{12} W .

Most (but probably not all) of the energy for torus emissions is supplied through pickup of neutrals. In the early 1980s, it had been assumed that pickup could supply all the energy (described in the literature as Neutral Cloud Theory). However, detailed calculations (Shemansky 1988, Smith *et al.* 1988) showed that T_e could not be maintained at a high enough level (because of inefficient ion–electron energy transfer through Coulomb collisions) to produce the observed emission and ion partitioning (Section 23.6). Hence, other energy supply mechanisms need to be invoked.

The emission rate per unit volume in the torus is around $1.1 \times 10^{-19} \text{ W cm}^{-3}$ ($0.67 \text{ eV cm}^{-3} \text{ s}^{-1}$). Ions at 100 eV at torus densities have about $3.2 \times 10^{-14} \text{ J cm}^{-3}$ of energy and thus the timescale for loss of this energy is around 3–5 days (Strobel 1989) which should be compared to the timescale for ion cooling by Coulomb collisions with electrons (estimated at 2–10 days) and the timescale for ion loss by radial transport (estimated at 20–80 days).

The emissions allow remote-sensing observations of torus properties and reveal that the structure is variable on many different timescales. Most of the processes producing this variability are poorly understood although there are clues to their nature. Some are probably related to features of Jupiter’s magnetosphere while others are almost certainly related to variations in the source. Given that the highly time-variable volcanic activity may contribute significantly to Io’s atmospheric structure, the latter might appear obvious. However, it has proved difficult to show a clear, unambiguous link between the two phenomena (Brown and Bouchez 1997).

Radial transport feeds heavy ions produced near Io into the rest of Jupiter’s magnetosphere (Section 23.7) and most of the phenomena exhibited by Jupiter’s magnetosphere depend on these ions. Little evidence of plasma is seen inside $5.0 R_J$ which may indicate an inner boundary. No similar boundary outside Io’s orbit appears to exist and therefore iogenic ions sputter and impregnate the surfaces of the outer Galilean satellites (in particular, Europa). This expansion of plasma into the middle magnetosphere is a significant mass loss process for the torus. Charge exchange (and subsequent ballistic escape) is also an important mechanism and leads to an observable cloud of neutrals which extends out to more than $400 R_J$ from Jupiter. The distribution of neutrals in this cloud has been used as a diagnostic of processes occurring back at Io’s orbit (Wilson *et al.* 2002).

The rest of this chapter describes in more detail the physical processes that lead to the observed properties of the Io plasma torus. The topics are approached by (i) describing the source and resulting phenomena, (ii) discussing the resulting spatial distribution of plasma torus, its composition and energy balance, (iii) looking at how mass is lost, and (iv) describing the time variability of the system. In doing so we address six key issues.

1. Where, in relation to Io, is most of the mass and energy injected into the torus?
2. Have we established all the energy sources and sinks?
3. How significant is the high energy tail of the electron distribution for torus composition and energetics?
4. What do we know about transport through the system and subsequent loss?
5. Is there a link between Io’s volcanic and/or atmospheric variability and torus conditions?

6. What else is variable in the system and what provokes this variability?

The chapter will show that we have ideas but that the details remain open for future research.

23.2 ESCAPE FROM IO

Io’s volcanically generated SO_2 atmosphere is constantly being lost to space by several processes. In Io’s atmosphere, solar ultraviolet photons and magnetospheric electrons ionize atoms and molecules which are then picked up and incorporated into the torus. These heavy ions in the torus in turn collide with neutrals in Io’s atmosphere, either ejecting them from Io via elastic collisions, or ionizing them by charge exchange collisions.

Molecules and atoms which are ejected as neutrals form neutral clouds around Io and Jupiter, and the morphology of each cloud component is a reflection of the atmospheric ejection mechanism which generates it. Although some fraction of atoms lost from Io’s atmosphere do not contribute directly to neutral cloud production (simple ionization and pickup into the torus), neutral clouds of one form or another are an inevitable result of the plasma torus/atmosphere interaction and atmospheric escape.

The neutral clouds of sodium are particularly useful for studying the Io/magnetosphere system. Atomic sodium is only a trace constituent of the atmosphere (\sim few %), but its large cross section for scattering visible sunlight (Chamberlain and Hunten 1987) makes it by far the most easily observed species in the neutral clouds. Atmospheric escape of the less visible sulfur and oxygen species can be inferred, to some extent, by analyzing the sodium clouds.

Observations and modeling of the sodium clouds at multiple spatial scales reveal the identities, rates, and energies of the major atmospheric escape mechanisms for sodium. Figure 23.3 shows two ground-based images and one space-based image of the sodium clouds near Io and around Jupiter. Close to Io, sodium atoms can be seen just after escaping from the atmosphere (Figure 23.3a). Further out and around Jupiter, energetically distinct cloud components are visible (Figure 23.3b). The giant “sodium nebula”, formed by atoms which are escaping from the jovian system, is visible at the largest spatial scale (Figure 23.3c). Figure 23.3d, covering the same spatial scale as Figure 23.3b, is a diagram of the major cloud components depicted from above Jupiter’s north pole.

There are two major categories of escape from Io – ionospheric and collisional. We discuss the evidence for these processes in turn.

23.2.1 Ionospheric Escape and “Fast” Neutral Clouds

Sodium Jet

During intermittent and extended periods, the electric fields associated with Jupiter’s magnetospheric interaction with Io rip ions out of Io’s collisionally thick ionosphere, forming a jet of sodium. The jet (Figure 23.3a and d) is a narrow cloud which extends from Io in a direction approximately away from Jupiter. Its direction oscillates over a period of several

IO SODIUM CLOUDS

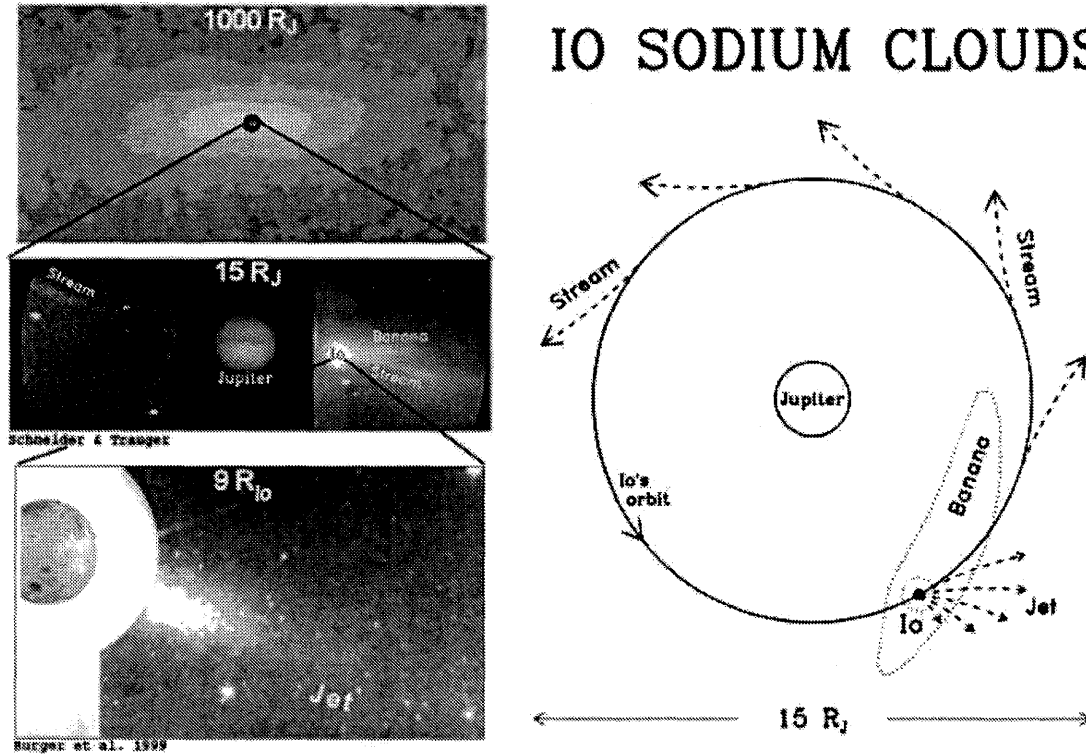
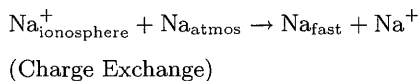
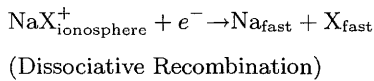


Figure 23.3. Left: Images of the neutral sodium clouds on three different scales. Top: The emission from sodium extending out to 500 R_J from the planet. This material has (mostly) escaped Jupiter’s gravitational field. Middle (b): The sodium stream seen in a ground-based image covering the orbit of Io. Bottom (c): The appearance of the sodium jet as seen by the *Galileo* imaging system. Right: A schematic of the sources of these sodium structures.

hours depending upon Io’s magnetic longitude (Pilcher *et al.* 1984) and always points approximately perpendicular to the local unperturbed magnetic field at Io (Wilson and Schneider 1999). This directionality relative to the magnetic field indicates that fresh pickup ions in a ring distribution (see below), either Na⁺ or unidentified molecular ions (NaX⁺), are being neutralized, with the resulting daughter Na atoms reflecting the cyclotron and drift velocities of the parent ions, i.e.,



or



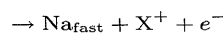
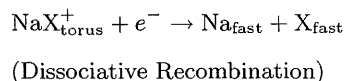
The exclusive anti-jovian directionality of the jet indicates that the electric field in Io’s ionosphere is forcing ions out the top of Io’s anti-jovian atmosphere, where charge exchange or recombination near the exobase can produce the fast neutrals for the jet. This current across Io is probably part of the current system connecting Io with Jupiter’s ionosphere (Figure 23.5) through Birkeland (magnetic field aligned) currents in Jupiter’s magnetosphere (e.g., Belcher 1987, Chapter 22).

Since ions in the ionosphere are flowing out of one side of Io’s atmosphere, it is plausible that some resident torus ions and newly created ions may be flowing into other regions of the ionosphere from outside, meaning the ionosphere is not

entirely populated by local ionizations. It therefore remains unclear how important various ionization mechanisms are for maintaining the ionosphere.

Sodium Stream

The sodium “stream” is a long, narrow cloud feature (Figure 23.3b and d) which leads Io in its orbit and which undulates above and below the centrifugal equator along its length with the same period as the jet. The stream is related to the jet in that it results from the neutralization of fresh, essentially corotating, pickup ions. The difference is that the ions which form the stream recombine in the torus a few hours after leaving Io’s vicinity, whereas it takes minutes or less for the jet-forming ions to recombine close to Io. Simple recombination of Na⁺ has a timescale of several hundred days, even in the densest regions of the torus. The timescales for production of Na in the stream must be ≤10 hours in order to produce such a clearly defined structure. Only molecular ions can recombine so quickly in the relatively rarified plasma torus, so the stream must be formed by NaX⁺ ions which have escaped from the ionosphere (Schneider *et al.* 1991), i.e.,



(Impact Dissociation)

It is possible that the jet is produced by the same escaping NaX^+ ions, meaning the jet may simply represent higher dissociative recombination rates in the part of the stream closest to Io, where plasma densities are greatest. The unidentified parent, NaX^+ , has not been detected by either remote or in situ means, but molecular ions of S and O species are obvious possibilities (Johnson 1994a). Ions of NaCl are also candidates given the discovery of Cl ions in the torus at concentrations similar to those of Na (Küppers and Schneider 2000, Moses *et al.* 2000, Feldman *et al.* 2001) and the detection of NaCl in Io's atmosphere (Lellouch *et al.* 2002). Potassium (first identified as a neutral cloud component by Trafton 1975) has also been detected spectroscopically near Io as part of either a stream or jet (Thomas 1996).

It is uncertain to what extent similar streams and jets of S and O exist. Photochemical equilibrium in a collisionally thick and static ionosphere would be dominated by Na^+ and K^+ because of their relatively low ionization potentials (Kumar 1985, Summers 1985, Summers and Strobel 1996, Moses *et al.* 2000), suggesting that if the jet is produced by escaping *atomic* ions, it may be unique to Na and K. On the other hand, in situ measurements by the *Galileo* spacecraft detected wave signatures at frequencies close to the gyrofrequencies of SO_2^+ and SO^+ near Io (Kivelson *et al.* 1996b, Warnecke *et al.* 1997), implying that molecular ion streams of S and O are probably present. The *Cassini* spacecraft found evidence of extended nebulae of S, O, and SO_2 escaping from the Jupiter system by detecting fresh pickup ions (including SO_2^+) in the solar wind well upstream of Jupiter (Krimigis *et al.* 2001). However, these probably result from charge exchange of S^+ and O^+ torus ions with the S and O “banana” clouds (as described below), a process which is not significant for sodium.

Numerical modeling of the jet and stream can be applied to the observations to determine ejection rates of Na and the velocity distribution of the parent ions. Figure 23.4 shows a comparison of stream and jet models with observations. The stream process ejects Na from the torus at rates of 10^{26} to 10^{27} atom s^{-1} , and NaX^+ ions must escape from Io with at least those rates to maintain the stream (Schneider *et al.* 1991, Wilson and Schneider 1994, 1999, Wilson *et al.* 2002). Ejection rates from the jet process are typically an order of magnitude lower than the stream (Burger *et al.* 1999, Wilson and Schneider 1999, Wilson *et al.* 2002). Gyrospeeds of the parent ions range from the magnetospheric corotation speed past Io of 57 km s^{-1} down to 20 km s^{-1} or less, indicating that the plasma flow speed relative to Io in the pickup region near Io is variable on timescales of a year or less. Unlike the jet, the parent ions forming the stream have a broad pitch-angle distribution, suggesting they have had time to be pitch-angle scattered by plasma waves (Wilson *et al.* 2002).

Our new understanding of the jet and stream processes has simplified the overall picture of Io's atmospheric escape and neutral cloud production. The jet entirely explains the “directional features” (Pilcher *et al.* 1984, Goldberg *et al.* 1984), and the “preferential-ionization shaping” mechanism (Pilcher *et al.* 1984) has now been ruled out by multi-scale observations and additional modeling. Charge exchange of thermal torus ions in Io's exosphere, once thought to be the dominant means of fast neutral Na ejection and Na neb-

ula production (Eviatar *et al.* 1976, Brown and Schneider 1981, Mendillo *et al.* 1990, Smyth and Combi 1991), is also no longer tenable as a major source mechanism. Instead, a high-gyrospeed, long lifetime stream appears to be the dominant fast sodium ejection process most of time (Wilson *et al.* 2002). It should be noted, however, that there is significant charge exchange of thermal S^+ and O^+ ions with S and O (Smyth and Combi 1988, Schneider *et al.* 1989), but this occurs mostly remote from Io rather than in Io's exosphere. It is also important to note that charge exchange between Na^+ and Na does happen in Io's atmosphere, but most of the ions are probably either ionospheric pickup ions or collisionally modified torus ions, so the resulting neutral clouds (the jet) have modified pickup energy signatures, rather than thermal ones.

23.2.2 Sputtering, Knock-on Collisions and Slow Neutral Clouds

The other major category of atmospheric escape involves elastic collisions of neutrals in Io's atmosphere with escaping ionospheric ions and impinging torus ions.

Knock-on collisions involve relatively close ion-neutral interactions that are capable of transferring sufficient energy to eject a target atom from Io's atmosphere with a single collision. The energy imparted to the target neutral depends on the impact parameter of the collision; lower energy transfers are more likely than higher ones.

Atmospheric sputtering involves a multi-step cascade of ion-neutral and neutral-neutral collisions which can ultimately eject several atoms and molecules from the atmosphere for each incident ion (Haff *et al.* 1981, McGrath and Johnson 1987, Johnson 1994b). This is analogous to surface sputtering, with the gravitational escape energy of each molecule in the atmosphere substituting for the binding energy of a molecule in a surface. The multiple collisions in the cascade are mostly low-energy “orbital” collisions (Brown *et al.* 1983b). Many of the neutrals involved in the collisions do not escape, resulting in a net heating and expansion of Io's upper atmosphere (Johnson 1989, Pospieszalska and Johnson 1992, Wong and Smyth 2000).

Since knock-on collisions and sputtering cascades result in mostly low-energy momentum transfers, most of the ejected neutrals escape at speeds of only \sim a few km s^{-1} . Hence, the neutrals form large clouds that extend approximately along Io's orbit, both ahead of Io and behind it. In addition to the sodium cloud (Figure 23.3b and d), clouds have been detected for sulfur (Durrance *et al.* 1983, 1995), oxygen (Brown 1981, Durrance *et al.* 1983, Thomas 1996), and potassium (Trafton 1981). These extended clouds are confined close to the rotational equator and therefore cross the densest regions of the torus every 6.5 hours. They are then subject to additional momentum-transfer collisions, electron impact dissociation (for molecules), and ionization by both electron impact and ion-neutral charge exchange. Ionization erodes the extended clouds, thus limiting their extension both ahead of and behind Io. The detailed shape of the Na cloud and the corresponding clouds of other species depend on a complex interaction of ejection, orbital motion, and ionization, so numerical modeling has been a critical tool for determining the ejection rates and speed

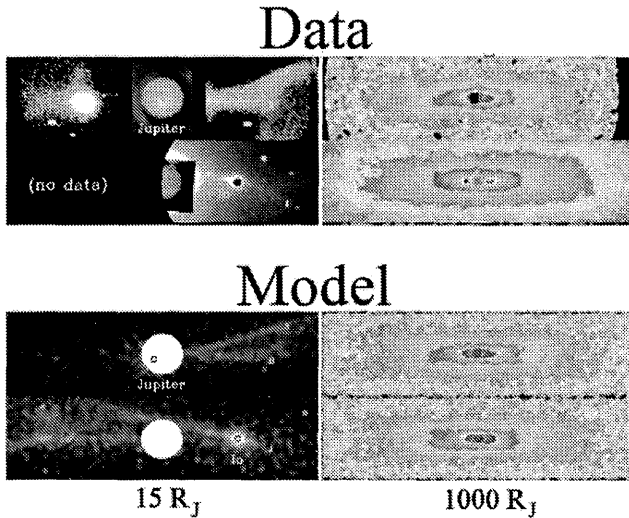


Figure 23.4. A comparison between observational data (top) and Monte Carlo models (below) of the ejection of sodium from Io.

distributions of the sputtering process from data (Smyth and Combi 1988). The resulting shape of the Na cloud resembles a banana. Sodium atoms ejected from Io at various angles have orbits with either more or less energy than Io's. Backwards-ejected atoms have trajectories falling towards Jupiter. Typically, sputtering ejects $\sim a \text{ few} \times 10^{26}$ Na atom s^{-1} from Io's atmosphere (Smyth and Combi 1988, Cremonese *et al.* 2000, Wilson *et al.* 2002). Sputtering rates of S and O species are thought to be at least an order of magnitude greater, in proportion with their greater abundances in Io's atmosphere (Smyth and Combi 1991, Smyth 1992, Smyth and Marconi 2000).

The timescales for loss of the neutral sputtered clouds vary depending upon the species. The minimum lifetimes against electron impact ionization for sodium, potassium and sulfur are relatively short (2–5 hours) in the densest regions of the torus. The rate coefficient for oxygen, however, is at least an order of magnitude smaller than for sulfur so that charge-exchange loss with torus ions is dominant. The minimum lifetime for O is around 20 hours (e.g., Thomas 1992) resulting in significant densities of neutrals remote from Io and a much more extended shape about Jupiter. Around 180° in Io phase away from Io itself, densities of neutral O and S were at least $29 \pm 16 \text{ cm}^{-3}$ and $6 \pm 3 \text{ cm}^{-3}$ respectively (Skinner and Durrance 1986). Lagg *et al.* (1998) have derived a density of 35 oxygen atoms cm^{-3} using measurements from the *Galileo* energetic particle detector. This value is effectively an average over Io's orbit. The $\mathbf{E} \times \mathbf{B}$ drift of the energetic particles smears out longitudinal asymmetries because the timescales for charge-exchange losses of energetic charged particles are in the order of the jovian rotation period (A. Lagg, personal communication). These neutrals can provide additional energy and mass to the torus remote from Io via charge exchange and/or electron impact ionization.

23.2.3 Torus Supply Rates

As noted in Section 23.1, the total mass loss from Io is widely assumed to be 1 ton s^{-1} but this value is not well constrained. There are effectively three source regions: (i) the cold, dense material in the wake of Io where the flow is almost stagnant, (ii) material ionized within a few Io radii of the satellite within the local interaction region (which would include material ripped out of Io's collisionally thick ionosphere, some fraction of which is neutralized to form the sodium jet), (iii) material ionized remotely from Io beyond a few Io radii (which would include ions produced from ionization of the “banana” cloud, for example). We can attempt to estimate the supply rates from each of these sources from the observations.

By using the density, flow speed, and cross-sectional area of Io's wake derived from *Galileo* measurements, the plasma production there must be relatively low ($< 10 \text{ kg s}^{-1}$).

The supply rate within a few Io radii is, by far, the most complicated to assess. Based on the *Galileo* J0 flyby data, values between about 0.3 and $1.7 \times 10^{28} \text{ s}^{-1}$ (Bagenal 1997, Saur *et al.* 2003), equivalent to 120–700 kg s^{-1} , have been suggested. Saur *et al.* (2003) have recently concluded that the supply rate must be at the lower end of the range. As Table 23.1 shows, while it is possible to observe the effects of ionospheric escape from the ground (e.g., the sodium jet) and while the existence of molecular ionospheric escape almost certainly implies that atomic escape is also occurring, the contribution to the mass and energy content of the torus from these mechanisms is extremely difficult to even estimate from ground-based data. We have indicated this in Table 23.1 by using question marks.

The material ionized remote from Io can, however, be assessed assuming that much of it is produced by atmospheric sputtering with subsequent ionization. This has been performed through modeling of the “banana” cloud (cf. Smyth 1992, Wilson *et al.* 2002). Table 23.1 shows that the total mass loss rate from Io through this mechanism is at least 971 kg s^{-1} . (Note, however, the assumption in Table 23.1 comment b. The observational constraints on the relative contributions of Na, O, and S to the remote neutral clouds are by no means strict.) Not all of the ionization occurs in the outer region because this calculation also includes sputtering within a few Io radii (in an admittedly non-self-consistent way because it does not model the currents generated through the pickup process, for example, which are highly significant at Io).

Smyth and Marconi (2003a,b) have recently adapted the model of Smyth and Combi (1988) to separate these inner and outer sources within the sputtering mechanism calculation. They concluded that 600–1000 kg s^{-1} was being ejected from the inner region and around 200 kg s^{-1} from outside a few Io radii. (The total from the modeled process agrees fairly well with Table 23.1.) Thus, the sputtering process alone appears to produce a local source 3–5 times higher than the remote source. MHD simulations (e.g., Combi *et al.* 1998, Linker *et al.* 1998) would generally support this but it is not in agreement with the assessment of *Galileo* data (Saur *et al.* 2003).

Hence, the assumption of a loss rate from Io of about 1 ton s^{-1} is probably justified (although the ionospheric es-

cape mechanism is ill-constrained) but the relative importance of the local interaction region and the remote region of ionization is not yet clear. However, it should be noted that the neutral distribution in the remote region is highly non-uniform irrespective of whether the local or the remote source dominates. This leads to a distribution of the ion supply rate to the torus in the remote region which is strongly peaked in the vicinity of Io and its orbit. This will be important in the following section.

Using a gyrospeed of 57 km s^{-1} , the total mass loss converts to a total energy supply of $1.6 \times 10^{12} \text{ W}$. This is comparable to the radiated energy loss but not all of the energy supplied is radiated. On the other hand, the net mass supply to the torus appears to be only about 40% of the total loss rate from Io (the remaining mass is lost from the system through charge exchange) or around 400 kg s^{-1} (see also Smyth and Marconi 2003b). The mass and energy balance issue will be discussed further in Section 23.6.

Finally, measurements of the deviation from corotation in the torus can also be used to estimate the total mass loading in the torus (Section 23.3, M. Brown 1994). Although the deviation from corotation can be measured rather accurately, the derivation of the total mass loading requires knowledge of the height integrated Pedersen conductivity of the jovian ionosphere, Σ , which is very poorly constrained. Brown expressed his result in the form $2\text{--}3 \times 10^3 \times \Sigma/0.03 \text{ kg s}^{-1}$ where Σ is in units of Siemens.

23.3 COROTATION AND MASS LOADING

Creation of fresh ions in the torus is followed by pickup and acceleration to near corotation. It is this process which provides the torus with much of the energy to balance the radiative losses. The corotation velocity at Io's orbit is just over 74 km s^{-1} . This should be compared with Io's orbital velocity (17.4 km s^{-1}) and therefore, the corotating plasma would pass Io at 57 km s^{-1} if unperturbed. The energy needed to accelerate the ions to these velocities is extracted from Jupiter's rotation. The coupling between the magnetosphere and Jupiter is provided by a Birkeland current system (Figure 23.5) which closes in Jupiter's ionosphere and enforces corotation of the magnetosphere (Bagenal 1989).

The production of new ions counteracts this. Essentially, the fresh ions screen out the corotation field. If there are sufficient numbers of fresh ions, corotation cannot be immediately enforced and lower velocities than corotation result. However, the process depends upon the spatial distribution of the ion source for which there are two viable hypotheses.

If the escape flux from Io were mainly in the form of neutral atoms or molecules, then the plasma source arising from electron impact ionization of this "neutral cloud" would be distributed all around Io's orbit, albeit with a strong concentration within a few R_{Io} of the satellite (e.g., Smyth and Marconi 1998). Alternatively, plasma created by electron impact ionization at the "top" of Io's gravitationally bound atmosphere (one or two scale heights above the exobase) may be stripped away immediately by the corotational flow, resulting in a plasma source that is tightly confined near Io (e.g., Cloutier *et al.* 1978). As we have seen in Section 23.2, both processes occur to some extent, but the question

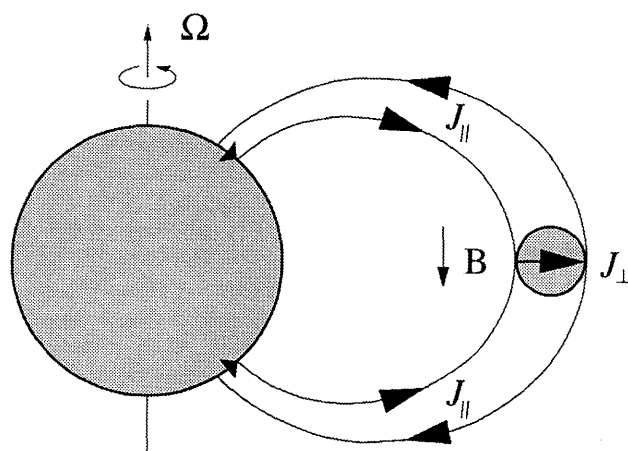


Figure 23.5. The Birkeland (J_{\parallel}) current circuit that delivers angular momentum from Jupiter (left) to Io (right), and to plasma created near Io. This is the classical "unipolar inductor" circuit first invoked by Piddington and Drake (1968) and Goldreich and Lynden-Bell (1969) to explain Io-controlled radio emissions from Jupiter. The equatorial current J_{\perp} is presumably a combination of pickup currents (Figure 23.6) and Pedersen conduction currents in Io's extended atmosphere. In Io's downstream wake, the current J_{\perp} is presumably instead the acceleration current that brings newly-injected plasma up to corotation. (For the sake of clarity, the sizes of Jupiter and of Io are exaggerated.)

of which, if either, provides the dominant plasma source remains open.

The process of direct stripping of ions from the top of the atmosphere was not actively pursued before the *Galileo* "J0" encounter with Io in December 1995, although work based on this type of model had begun in order to explain structures seen in neutral sodium emissions (Wilson and Schneider 1996, Thomas 1996). Results from that encounter, however, call for a re-appraisal of the direct stripping process. In the corotational wake region immediately downstream of Io ($1.5 R_{Io}$ from Io's center), the ion density exceeds that in the surrounding torus by an order of magnitude (Frank *et al.* 1996, Kurth *et al.* 1996). The corotational flow is almost completely stagnated there (Frank *et al.* 1996) and the magnetic field perturbation is comparable in magnitude to Jupiter's background field at that location (Kivelson *et al.* 1996a). Ion cyclotron waves, which are diagnostic of the ion pickup process (see below), are also strongly peaked at this location (Kivelson *et al.* 1996b) and field-aligned beams of hot electrons (which may provide an additional ionization source) were also detected (Williams *et al.* 1996, Williams *et al.* 1999, Frank and Paterson 1999). The strength of this interaction was not anticipated, and is difficult to explain unless a significant fraction ($\sim 1/2$) of the total torus mass loading occurs very near Io. The location of the plasma source has consequences both for the temperature of the torus and for its stability and dynamics.

The temperature effect is a result of the ion pickup process illustrated in Figure 23.6 (Goertz 1980). When an atom or molecule is ionized by electron impact or by photoionization (the former being more frequent in the Io torus environment), the resulting positive ion and electron are initially accelerated outward and inward, respectively, by the $E = -v \times B$ electric field associated with the local plasma

Table 23.1. Estimates of the mass loss rates from Io and the supply rates of mass and energy to the torus from ground-based observations.

Process	Molecular Ionospheric Esc.		Atomic Ionospheric Esc.			Atmospheric Sputtering → ionization (b)			Totals
	NaX ⁺	SO ₂ ⁺	Na ⁺	S ⁺	O ⁺	Na	S	O	
Species	NaX ⁺	SO ₂ ⁺	Na ⁺	S ⁺	O ⁺	Na	S	O	
Atomic Wt.	58(NaCl)	64	23	32	16	23	32	16	
Loss rate (10 ²⁶ s ⁻¹)	>6(a)	~10(?)	?	?	?	3	90	180	>289
Loss rate (kg s ⁻¹)	>58	106	?	?	?	11	480	480	>1135
Fraction of loss added to torus	0–50%		0–100% (d)			90%	50%	30%	
Mass Rate to torus (kg s ⁻¹)	0 to ~60	0–53	?	?	?	10	240	144	394–507
Mass Rate contributing energy to torus (kg s ⁻¹)	0 to ~60	0–53	?	?	?	11	480	480	971–1084
Energy Rate to torus (10 ¹¹ W) (c)	0 to ~1	0–.86	?	?	?	0.17	7.8	7.8	15.8–17.6

(a) Lower limit of loss rate for NaX⁺ is an average rate from Wilson *et al.* (2002), assuming that 100% of NaX⁺ ions yield the observed escaping Na atoms by dissociative recombination. In that case, there is no mass or energy added to the torus. However, if electron impact dissociation results in fewer than 100% of NaX⁺ yielding fast Na, then the NaX⁺ escape rate is higher, and the ion fragments do then add mass and energy to the torus. Upper limits of mass and energy rates assume twice the minimum escape rate – i.e., half of NaX⁺ ions yield fast Na.

(b) Sputtering rates of S and O are scaled up from the total loss rate of Na (sputtered Na and escaping NaX⁺), assuming total atmospheric loss rates scale as 1:10:20 for Na, S, and O, respectively (Schneider *et al.* 1989, Smyth and Marconi 2002).

(c) The energy input rate to the torus assumes a gyrospeed of 57 km s⁻¹ for escaping ionospheric ions, and a pickup speed of 57 km s⁻¹ for sputtered atoms which are ionized in the torus.

(d) Ionospheric escape of molecular ion species implies escape of atomic ion species as well, but there are no data which would provide direct estimates of escape rates. If Io’s ionosphere is created by torus ions which have entered Io’s atmosphere, then atomic ion escape contributes essentially no mass to the torus, because atomic ion chemistry simply changes the identity of the ions before they re-join the torus. If, however, electron impact ionization (with some photoionization) produces the ionosphere, then atomic ion escape does add mass to the torus.

Molecular ion escape rates from Kivelson *et al.* (1996) and Warnecke *et al.* (1997).

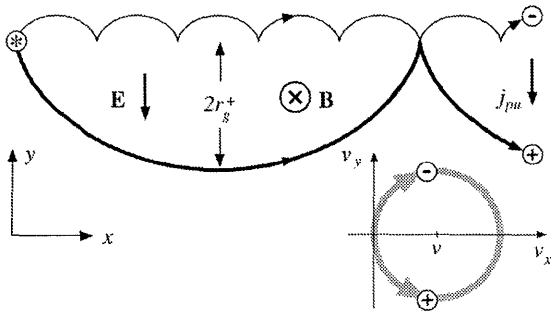


Figure 23.6. The pickup process. Top: Ion and electron trajectories following ionization at (*). The view is of the equatorial plane, with Jupiter to the top. For this illustration, the ion-to-electron mass ratio (hence gyroradius ratio) is taken to be 5 for clarity. In the Io torus, this ratio is $\sim 10^4$ (3×10^4 for O⁺, 6×10^4 for S⁺). Bottom: The resulting “ring” velocity distribution.

flow, ν , measured in the frame of reference in which the atom or molecule is initially at rest (essentially the Kepler orbiting frame). If \mathbf{E} and \mathbf{B} are uniform on the scale of one gyroradius $r_g = m\nu/qB$, the subsequent motion is a cusped cycloid, the sum of the uniform drift velocity ν and a circular gyration about \mathbf{B} with the same speed ν . The “pickup” velocity distribution is thus a delta-function ring in the $\nu_x - \nu_y$ plane with radius ν , centered at $(\nu_x, \nu_y) = (+\nu, 0)$, where x and y are as defined in the figure. The implicit assumption that

ν is large compared to the thermal velocity after the ionizing collision is probably good for ions but not for electrons. Pickup ions with ring distributions were directly observed in the near downstream region at Io (Frank and Paterson 2000b, 2001a).

Subsequent transport will alter both the drift velocity and the gyration (“thermal”) speed, but in fundamentally different ways. The drift velocity ν will follow the local flow field, which can change dramatically on short spatial scales $\sim R_{Io}$ (Figure 23.7). The gyration speed ν_{\perp} , however, is constrained by conservation of the first adiabatic invariant $\mu = m\nu_{\perp}^2/2B$, and thus changes much less dramatically on this scale. All torus ions, wherever created, end up almost corotating with Jupiter (see below), but their superimposed gyration speed (perpendicular thermal speed) depends sensitively on where they are created. Ions created in the relatively undisturbed corotational flow (e.g., point A in Figure 23.7) will have $\nu_{\perp} \approx \Omega r - v_K \approx 0.77 \Omega r$, where $\Omega \approx 2\pi/(10 \text{ hr})$ is Jupiter’s spin rate, r is distance from Jupiter’s spin axis, $\Omega r \approx 74 \text{ km s}^{-1}$ at $r = 5.91 R_J$, and $v_K \approx 0.23 \Omega r$ is the Kepler orbital speed at Io’s orbit. On the other hand, ions created in regions of nearly stagnated flow ($v \ll \Omega r$), e.g., points B and C in Figure 23.7, will have $\nu_{\perp} \ll \Omega r$. Ions created on Io’s flanks (point D) have $\nu_{\perp} > \Omega r - v_K$ by a factor of perhaps 2.

The initial temperature of torus ions is thus diagnostic of where they were created (Schneider and Trauger 1995). The observed low T_i in the torus ($\sim 100 \text{ eV}$) relative to the corotation energy therefore allows a range of possible ini-

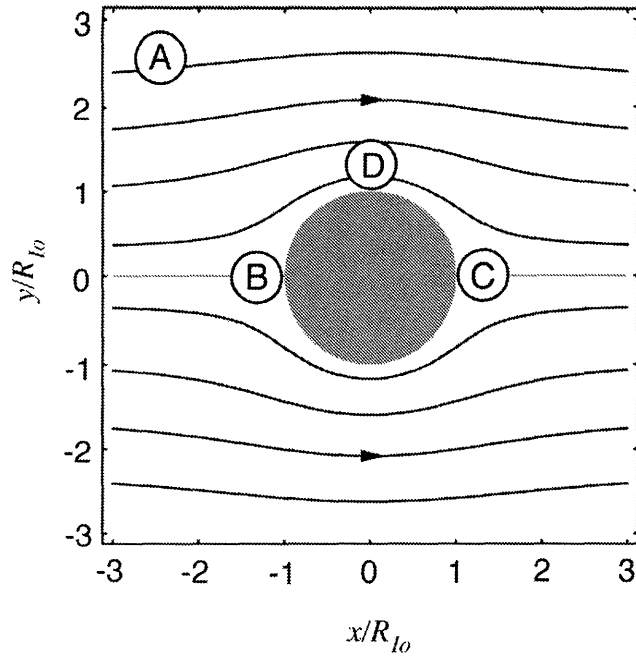


Figure 23.7. Sketch of the flow field around Io, as viewed in the equatorial plane. Ions created from neutrals moving with low velocity with respect to Io (in regions of relatively undisturbed flow, A) acquire thermal speeds $\sim 57 \text{ km s}^{-1}$, the speed of Io relative to the corotating frame. Ions created in the upstream (B) and downstream (C) stagnation regions acquire much smaller thermal speeds, while ions created on the flanks (D) acquire larger thermal speeds. In each case the acquired thermal speed is essentially the local plasma flow speed.

tial temperatures. If the ion residence time in the torus is short, the low T_i might indicate significant pickup in the upstream and downstream stagnation regions. If the residence time is long, cooling via Coulomb collisions with electrons occurs and consequently the mean initial temperature must be higher. This illustrates the importance in determining the residence time. Given the observed T_i we can estimate (assuming the residence time is zero) that the source, in stagnation regions cannot be more than about 3 times the extended neutral cloud source, but this limit is not particularly useful since the observed source in the stagnation region is $\leq 20\%$. Conversely, the low bulk T_i can certainly “hide” fresh, low pickup energy ions.

The effect of the flow field on the production rate is qualitatively as described above – for a given volumetric production rate in a homogeneous system, a given flux tube gains the most mass in regions where it spends the most time. The inverse effect (that of the production rate on the flow field) involves the “pickup current” density

$$j_{\text{pu}} = \frac{\dot{n}m}{B^2}E \quad (23.1)$$

which flows in direct consequence of the initial displacement of each new ion and electron by one gyroradius as described above. Here \dot{n} is the production rate of ion–electron pairs per unit volume per unit time, and m is the sum of ion and electron masses. If more than one ion species is produced, a summation over species is implied. Note that Eq. 23.1 is equivalent to Ohm’s law with an effective Pedersen conduc-

tivity $\sigma_{\text{pu}} = \dot{n}m/B^2$ in Io’s reference frame. Thus any actual Pedersen conduction current in Io’s atmosphere will simply add to the local pickup current (but without adding mass), as will charge-exchange reactions that replace a slow atom and a fast ion with a fast atom (which escapes) and a slow ion (which requires acceleration up to ν).

The pickup current, along with any associated Pedersen current in Io’s atmosphere, is closed by a Birkeland current. This is, in turn, closed by a Pedersen current in Jupiter’s ionosphere (Figure 23.5) which extracts angular momentum from the neutral atmosphere at the rate required to spin up the newly created plasma in the torus.

Although, the current structure is quite complicated owing to the inhomogeneity of the background plasma (e.g., Neubauer 1980, Pontius 2002), the ultimate closure of this current in Jupiter’s atmosphere is guaranteed by causality (because Jupiter is the ultimate source of angular momentum for torus plasma). Alternatively, Delamere *et al.* (2003a) argue that the field-aligned potential may limit the momentum transfer between Jupiter and the plasma. The electric field \mathbf{E} , when mapped along \mathbf{B} to Jupiter’s ionosphere and transformed to the reference frame of Jupiter’s atmosphere, must drive a Pedersen current that closes the pickup and Pedersen currents near Io. This is how the plasma production affects the electric field and associated plasma flow. The circuit (Figure 23.5) is equivalent to the unipolar inductor circuit proposed by Piddington and Drake (1968) and Goldreich and Lynden-Bell (1969). The only difference is that the conduction current at Io has been replaced, at least in part, by a pickup current (Eq. 23.1) which is equivalent to a conduction current in its electrodynamic effects.

The closure of the pickup current in Jupiter’s ionosphere requires a certain corotation lag (plasma rotation frequency $\omega < \Omega$) wherever new plasma is being produced (or replaced with non-corotating plasma through charge exchange). A complete description of this corotation lag would require a self-consistent model of the near-Io flow field and mass loading rate, which is not available (cf. Linker *et al.* 1998). It is, however, clear that a given mass-loading rate produces a larger corotation lag if it is confined to a smaller radial distance range. For example, if we assume an azimuthally-uniform mass loading rate, \dot{M} (kg s^{-1}) distributed uniformly between $r = L_s R_J$ and $(L_s + \Delta L)R_J$ ($L_s \approx 6$), then the corotation lag (Pontius and Hill 1982, Hill and Pontius 1998) is

$$R_J L_s \delta\omega = \frac{\nu}{1 + k\Delta L} \quad (23.2)$$

where $\nu = 57 \text{ km s}^{-1}$ is the speed of Io relative to the corotating frame, and

$$k \equiv \frac{4L_0^4}{\xi L_s^5} \quad (23.3)$$

$$\xi \equiv \frac{\dot{M}}{M_t} \sim 3 \quad (23.4)$$

$$L_0^4 \equiv \frac{\pi \Sigma B_J^2 R_J^2}{M_t} \quad (23.5)$$

In these definitions, \dot{M}_t is the rate of outward plasma mass transport from the torus, and is less than \dot{M} by a factor ~ 3 because charge-exchange reactions contribute to the latter but not the former (Pontius and Hill 1982). The quantity L_0 is the characteristic distance (normalized to R_J)

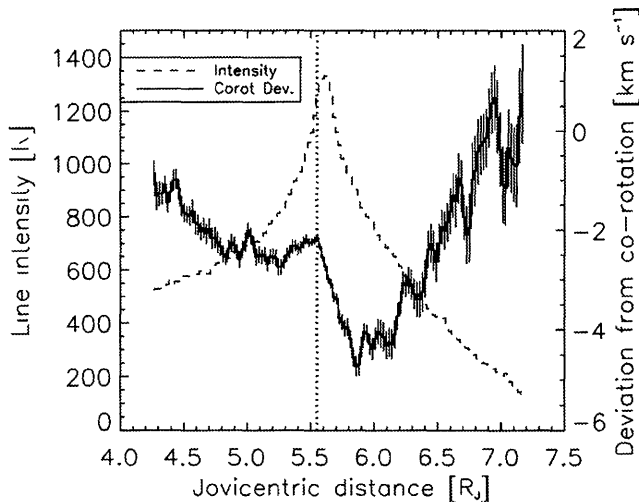


Figure 23.8. The Doppler shift of the S^{2+} 953.1 nm line has been used to derive the deviation from corotation in the torus as a function of radial distance (solid line with error bars). The plasma is slowest near Io's orbit but the slow down covers at least $0.4 R_J$ in radial distance. The observed intensity of the line is overplotted (dashed line, left scale). Note that no correction for line of sight effects has been made so that data points inside about $5.5 R_J$ do not reflect true torus conditions at those radial distances. Figure from Thomas *et al.* (2001).

at which corotation begins to break down in the outward-moving plasma (Hill 1979) (Σ is Jupiter's effective Pedersen conductance and B_J the strength of its surface magnetic field due to the dipole moment, at the dipole equator). The reason for this lengthy string of definitions is that neither Σ nor \dot{M}_t is well constrained by observations, but their ratio in Eq. 23.5 is constrained by the *Voyager 1* plasma flow observations (McNutt *et al.* 1979) that indicate $L_o \approx 20$ (Hill 1980). Thus, using $L_o = 20$, $L_s = 5.91$, and $\xi = 3$ gives $k \approx 30$ in Eq. 23.2.

If the mass loading is spread (more or less) uniformly over a substantial fraction of the radial width of the torus ($\sim 0.5 R_J$, Figure 23.8) then $\Delta L \sim 1/2$ and Eq. 23.2 gives a corotation lag $R_J L_s \delta\omega \sim 3.8 \text{ km s}^{-1} = 6\%$ of the corotation speed at $L = 5.91$. This result (Pontius and Hill 1982) is consistent with the broadly distributed corotation lag determined from spectroscopic measurements as described below. If we instead set $\Delta L \sim R_{Io}/R_J \approx 1/39$, Eq. 23.2 gives $R_J L_s \delta\omega \sim 0.57\nu = 32 \text{ km s}^{-1}$, corresponding to a 50% corotation lag and a 44% slowing of the plasma flow past Io. This is consistent with flow measurements during *Galileo's* Jupiter Orbit Insertion (JOI) pass near Io (Frank *et al.* 1996), except for the single measurement of almost complete stagnation immediately downstream, which may have been in the collisionally bound ionosphere.

Spatially resolved spectra of the Doppler shift of S^+ emission from the torus have been acquired remote from Io by several observers. These measurements are in good agreement showing deviations from corotation of up to 6% (cf. R. Brown 1983, M. Brown, Thomas *et al.* 2001). Figure 23.8 is an example which shows the deviation from corotation to have a radial extent of $\leq 0.4 R_J$ near Io's orbit. Both the *Voyager* PLS experiment and the *Galileo* plasma in-

strumentation (*Galileo* PLS) gave similar results. *Voyager 1* gave deviations of 0 to 6% in the region between 5.5 and 5.9 R_J (Bagenal 1985) while *Galileo* PLS measured deviations of 2–10% (Frank and Paterson 2001b).

The agreement between the theoretical corotation lag and its observed magnitude and radial extent can be interpreted as evidence in favor of the idea that mass loading is spread broadly through the torus. However, the observed lag may also result from the “atmospheric flywheel” effect (Pontius 1995); the subrotation of Jupiter's upper atmosphere in response to the time-integrated forcing by a localized but moving mass-loading region near Io. Thus, we have the happy (or unhappy) situation that corotation lag measurements are theoretically consistent with either most of the canonical 1 ton s^{-1} being injected broadly throughout the torus, or most of it being injected very close to Io, or indeed comparable amounts of both. (Complete stagnation in Eq. 23.2 would require $\Delta L \ll R_{Io}/R_J$, which may be plausible in an atmospheric stripping scenario.)

The Birkeland current circuit (Figure 23.5) that closes the pickup (and Pedersen) currents near Io is no doubt responsible at least in part for the bright auroral spot at the jovian footprint of Io (Connerney 1993, Chapter 26). The less bright but equally distinctive auroral trail that extends at least 90° of longitude downstream of the Io footprint (Clarke *et al.* 1998, Chapter 26) probably involves a similar current system, but not pickup currents *per se*. (There is no reason to expect a distribution of un-ionized source material to be confined tightly to Io's downstream corotational wake.) Instead, the equatorial part of the current system in the wake is probably the acceleration current required to enforce corotation (less the background 3%) on the flux tube that has interacted with Io and is still lagging behind corotation. The timescale for this acceleration must be at least $\sim 1 \text{ hr}$ to account for the observed length of the auroral tail. This timescale is plausible especially if a significant fraction of the circuit voltage ($\sim 500 \text{ kV}$) is dropped along the field lines (Hill and Vasyliunas 2002, Delamere *et al.* 2003a, Su *et al.* 2003). The implication would be that an identifiable corotational wake exists at least 90° downstream of Io.

23.4 LATITUDINAL AND RADIAL STRUCTURE OF THE TORUS

23.4.1 Ion and Electron Temperatures

In Figure 23.9, radial profiles of S^+ emission and T_\perp through the torus are shown. It can be seen that just outside Io's orbit (typically at $6.0 R_J$) T_\perp is at a maximum. This maximum is often around 100 eV but it is strongly dependent upon the System III longitude of the observation with variations by a factor of 2 being usual. For comparison, the *Galileo* PLS gave $T_i \sim 70 \text{ eV}$ at $6.0 R_J$ during both the I24 and I27 orbits at a System III longitude (λ_{III}) $\sim 90^\circ$ (Frank and Paterson 2001a). (As noted in Section 23.1, there is no strong evidence for significant anisotropy and hence, T_i can be compared with T_\perp .) As one moves radially outwards into the warm outer torus, T_i , n_e , and the densities of ion species, such as S^+ (n_{SII}), slowly decrease. As one moves towards Jupiter, however, the peak n_e (and n_{SII}) initially rises rapidly while T_i drops. This is the ribbon. Finally, as

one moves closer still to Jupiter, T_i drops further to values below 10 eV, n_e and n_i drop rapidly but rise slightly again to form a secondary maximum which characterizes the cold torus.

The temperature structure closely resembles that found using the *Voyager 1* PLS experiment (Bagenal 1994) which is superimposed upon Figure 23.9. The discrepancy between the two measurements inside 5.2 R_J is probably caused by T_i dropping to such low values that the line was no longer resolved by the ground-based Doppler measurements used for this illustration. The value of T_\perp inside 5.2 R_J therefore would constitute an upper limit.

Outside 6.5 R_J , the discrepancies are less straightforward. As the torus ions diffuse outwards, there is expansion and one therefore expects cooling. They also continue to radiate and hence cool further. Ground-based spectra of S^+ (e.g., Thomas et al. 2001) and *Voyager 1* UVS measurements (Herbert and Sandel 1995) seem to show a general cooling with distance consistent with this concept. The decrease in T_i for ions at the centrifugal equator appears to be consistent with an L^{-3} law although the error bars on the exponent are large. (An $-8/3$ exponent is appropriate for 3-D expansion of an isotropic plasma that fills the whole flux tube. The -3 exponent is more appropriate here for 2-D expansion of a plasma that is confined to a constant scale height. n and T_\perp are both proportional to B in this case.) *Voyager 1* PLS measurements showed an increase in T_\perp with distance but these observations were acquired out of the plane of the centrifugal equator, which, when combined with non-Maxwellian distributions, probably led to higher measured temperatures (see, e.g., Thomas and Lichtenberg 1997). However, the picture may not be quite so simple. For example, Doppler-resolved measurements of S^{2+} seem to show a constant T_i through the warm torus (e.g., Thomas et al. 2001).

Furthermore, *Voyager 1* PLS measurements (Belcher 1983) show temperatures broadly constant or slightly rising at distances greater than about 7 R_J , as one moves into the middle magnetosphere, suggesting the presence of an additional energy source. Candidate mechanisms include fresh pickup from extended neutral clouds, ionization of fast neutrals, and inward diffusion of hotter plasma from the middle and outer magnetosphere.

There is no evidence of ions at pickup temperatures in the bulk torus close to Io (although they were detected by *Galileo* PLS near Io; Frank and Paterson 2002). As noted in the previous section, either the ions are picked-up at the observed temperature (60–100 eV) or the amount of material is so small that it is “hidden” by the torus plasma along the line of sight. The latter seems much more probable because there is no fixed source position (in magnetic coordinates) into which pickup ions are continuously injected. The pickup ions are distributed over a range of L -shell. Furthermore, it appears that the timescales are such that the injected mass per unit volume per second must be small compared to the torus density and the transport time is roughly comparable to the cooling time (Strobel 1989) needed to get from pickup energies to about 60 eV. However, detailed 3-D modeling still has to be performed (see Section on NCT).

T_e was measured by *Voyager 1* (Sittler and Strobel 1987) and has a far simpler structure – it steadily increases from less than 1 eV in the cold torus, reaches around 4–5 eV

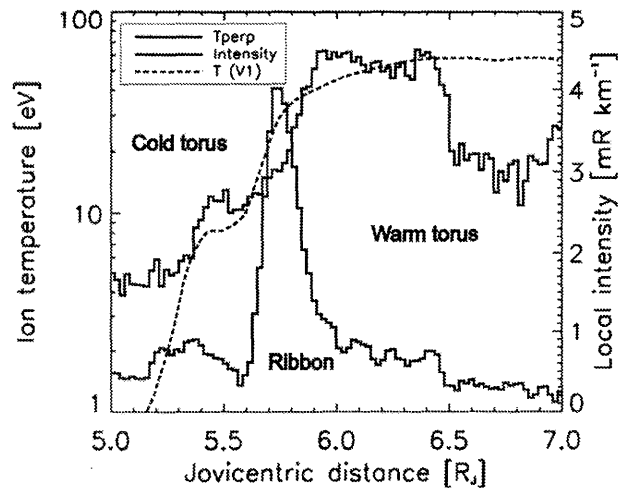


Figure 23.9. Radial profile along the centrifugal equator of the dusk ansa of the Io plasma torus in S^+ (673.1 nm emission) after processing to remove effects from the line of sight. The ribbon is prominent as the narrow spike of emission at around 5.7 R_J . Superimposed upon this is the derived ion temperature. Notice the sharp drop from the maximum near Io’s orbit inwards to the cold torus at 5.3 R_J . (This observation was acquired in October 1999 using the European Southern Observatory’s 3.5 m New Technology Telescope.) The dotted line is T_i as measured by the *Voyager 1* spacecraft during its fly-through in March 1979.

near Io’s orbit and continues to increase until reaching values near 8 eV near the orbit of Europa. *Galileo* PLS measurements of the core electron temperature (Frank and Paterson 2000a) during JOI show similar behavior (although the torus appeared to be denser at JOI than later in the mission).

Ground-based observational evidence to support this is difficult to acquire and to assess. At optical wavelengths, the S^+ 406.9 nm to 673.1 nm line ratio is diagnostic of T_e . However, the 406.9 nm and 407.6 nm doublet is around a factor of 10 fainter than the red, electron density sensitive, doublet at 671.6 and 673.1 nm. Line ratios in the UV are more promising but are more sensitive to the tail of the electron energy distribution which is known to be non-Maxwellian (Belcher 1983). We shall return to this issue in Section 23.5.1.

23.4.2 Latitudinal Distribution

The equilibrium position of a cold ion on a field line in a rapidly rotating magnetosphere is the point at which the field-aligned component of the centrifugal force vanishes. Assuming a tilted dipolar magnetic field for Jupiter, the equilibrium positions define a plane (the centrifugal equator) which is tilted by roughly 2/3 of the tilt of the magnetic equator with respect to the rotational equator (Hill et al. 1974, Siscoe 1977, Cummings et al. 1980). Ground-based imaging of the torus (Figure 23.10) agrees with this. The hotter the injected ion, the closer the equilibrium position is to the magnetic equator (Cummings et al. 1980).

Collisions produce pitch-angle scattering and equilibrate the ions over timescales of 1–30 days depending upon their initial energies (Strobel 1989). The temperature at which they equilibrate is a balance between energy input (via pickup and other energy input mechanisms), radiation losses, and mass losses (via charge exchange or expansion

losses which also remove energy from the system). The ion distribution approaches a scale height distribution given by

$$n_i \approx n_0 e^{-z^2/H_i^2} \quad (23.6)$$

where

$$H_i = \sqrt{\frac{2k(T_{i\parallel} + Z_i T_e)}{3M_i \Omega^2}} = 0.64 \sqrt{\frac{T_i(1 + Z_i C)}{A_i}} R_J \quad (23.7)$$

where Ω is the angular velocity, n_0 and n_i are the densities at the equilibrium position and at height, z , respectively, M_i is the effective ion mass, $C = T_e/T_i$, and Z_i is the average charge state (Hill and Michel 1976, Bagenal and Sullivan 1981). A more accurate description of the latitudinal distribution can be obtained by solving the diffusive equilibrium equation for a multi-species plasma incorporating an ambipolar electric field (Bagenal 1985). The method requires knowledge of the density of each species and $T_{i\parallel}$ at one point on each field line. In principle, the *Voyager* PLS and UVS measurements gave a fair description of these quantities (see below) and hence the 2-D distribution of plasma was derived (Bagenal 1994).

Previously, a single $T_{i\parallel}$ on each field line had been assumed but observational evidence (Herbert and Sandel 1995, Thomas and Lichtenberg 1997) suggests that this is no longer tenable and a polytropic relationship of the form

$$T_i \propto n_i^{-0.4} \quad (23.8)$$

has been suggested (Thomas and Lichtenberg 1997). The PLS data are now being re-interpreted using a so-called Kappa distribution (Vasyliunas 1968). Incorporation of a Kappa distribution into the diffusive equilibrium equations is fairly straightforward and improved descriptions of the spatial distributions of the major species in the torus have been presented (Moncuquet *et al.* 2002).

23.4.3 The Ribbon

The radial brightness in ground-based observations of the torus is usually dominated by the ribbon (Figure 23.10). Typically, the brightness of the S^+ 673.1 nm emission from this region is about 1 kR (1 Rayleigh (R) = $10^6/4\pi$ photon $\text{cm}^{-2} \text{sr}^{-1} \text{s}^{-1}$, Brown *et al.* 1983). Similarly, S^{2+} 953.1 nm emission peaks at this position and is typically 1.5 kR.

The structure seen in Figure 23.10 is the one most often seen but there are occasions when the ribbon is fainter than the cold torus (e.g., Jockers *et al.* 1992). However, the two major spacecraft fly-throughs of the torus have both prompted questions concerning this structure. The *Voyager 1* PLS measurements clearly identified a maximum in (inferred) n_e near 5.7 R_J . On the other hand, based on collisional excitation calculations (see below) the peak was not as strong as often indicated by ground-based observations (although curiously, ground-based observations of O^+ emissions from this region are normally fainter than predicted by models based on *Voyager* data). Thus the *Voyager 1* passage must have been at a time when the ribbon was fairly weak and the torus as a whole, oxygen-rich (Thomas *et al.* 2001).

The *Galileo* PLS measurements from December 1995

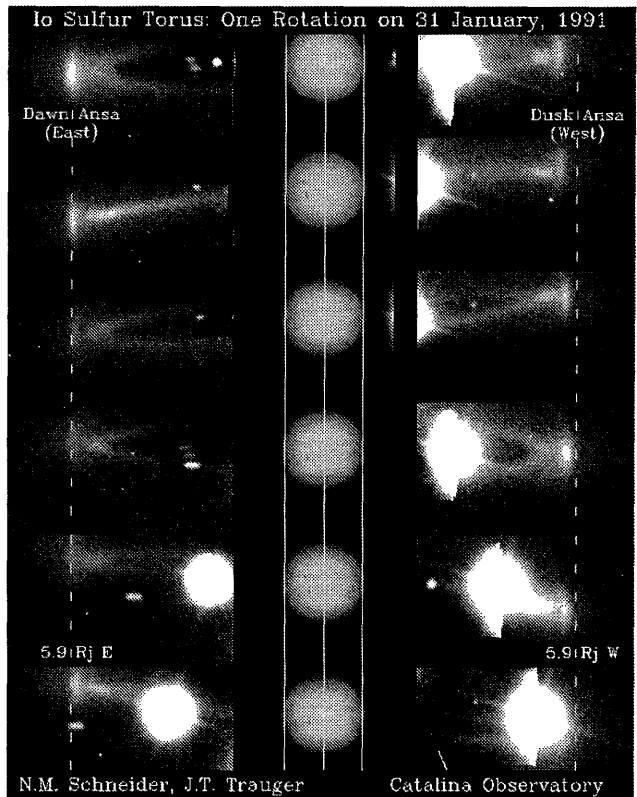


Figure 23.10. The changing appearance of the torus over one jovian rotation. On the dawn ansa, the bright ribbon feature is near the orbit of Io. On the dusk ansa, the ribbon is well inside Io's orbit. One can also notice (2nd frame from the top) the offset between the cold torus and the ribbon at the dusk ansa which suggests that the ribbon is offset from the centrifugal equator. From Schneider and Trauger (1995).

are even more perplexing (Bagenal *et al.* 1997) since either the ribbon was not present at all, or it had moved radially outwards to the orbit of Io (where its presence would have been concealed during *Galileo* JOI by Io itself). Hence, we have relatively few constraints on the properties of this structure from in situ measurements.

Imaging from the ground (Schneider and Trauger 1995) shows that the ribbon is closer to Jupiter on the dusk ansa while on the dawn ansa it is rather close to the location of Io's orbit. The presence of this maximum in ion density inside the orbit of the source is not well understood but recent work suggests a possible explanation.

It has been noted (Schneider *et al.* 1997) that the flux tube content is peaked in the ribbon. The peak in the flux tube content should be at the position of the source and, hence, some means of transporting material to positions inside Io's orbit have been discussed. However, it is also evident that the ribbon feature on the dawn ansa is at the same distance as Io's orbit (Schneider and Trauger 1995). These observations have led to the proposal that the formation of the ribbon is the result of an essentially continuous input at Io combined with the tilted dipole, a dawn-dusk electric field (produced by downtail plasma flow; see Section 23.4.6), and a diffusion coefficient which is strongly dependent upon radial distance (Herbert 1996, Smyth and Marconi 1998).

The concept requires an enhancement of ion injection

into the torus in the immediate vicinity of Io. At the dusk ansa, the ions are injected on drift paths extending to higher L values because of the dawn–dusk electric field. These ions are removed outwards into the middle magnetosphere quickly because the outward transport rate increases rapidly with L -shell. At the dawn ansa, the ions are injected on lower- L drift paths and remain on these drift paths much longer because the radial transport rate is much slower here. Thus, at 5.9 R_J on the dawn ansa, there is a build-up of material. When the torus rotates, the material at 5.9 R_J on the dawn ansa is brought in to 5.6 R_J at the dusk ansa (again because of the dawn–dusk electric field). Hence, the torus appears closer to Jupiter on the dusk ansa. The brightness is also higher there because the plasma is compressed as it moves closer to Jupiter. The offset of the tilted dipole acts to perturb this picture only slightly.

The geometry of the ribbon can be modeled (Herbert 1996, Smyth and Marconi 1998) under the assumptions that the plasma source is strongly peaked near Io's orbit and that the radial transport rate is much larger outside Io's orbit than inside. In these models the radial transport is represented by a radial diffusion coefficient that drops precipitously just inside Io's orbit. This transport model is probably oversimplified (see Section 23.7), but the basic idea is plausible. It has also been suggested that the ribbon is the downstream corotational wake of Io (Hill and Pontius 1998), a suggestion that retains the geometrical features of the above models subject to the same requirement that the radial transport rate be strongly suppressed inside Io's orbit.

In Figure 23.8, one can see that the peak ion density appears to be just inside the region of maximum deviation from corotation. Hence, it may be possible that it is the corotational wake of Io which is acting to reduce the radial transport rate leading to the observed position of the emission peak.

23.4.4 Cold Torus

Ground-based imaging and spectroscopy clearly show the presence of significant quantities of S^+ closer to Jupiter than the ribbon (e.g., Figure 23.9). *Voyager* PLS data show this region (the cold torus) to be characterized by low T_e and T_i (~ 1 – 2 eV; Bagenal 1985). S^+ emission from this region can, on occasions, dominate the emission from the ribbon but it is usually assumed that this is because of strong variation in the ribbon rather than any significant variability in the cold torus. Typical S^+ 673.1 nm emission levels are of the order of 400 R. The cold temperatures (which can also be inferred from the extremely low S^{2+} 953.1 nm emission from this region) suggest that the plasma has radiated most of its energy away and has become strongly confined to the centrifugal equator.

The *Galileo* PLS appears to have detected the rise in n_e towards the cold torus (and the accompanying sharp drop in T_i) during the JOI pass in December 1995 (Frank and Paterson 2001b). However, the measured n_e is around a factor of 5 lower than one would expect from *Voyager 1* PLS results. Given that ground-based observers show the cold torus to be far less variable than the ribbon, and that their results agree rather well with radiation calculations based on the *Voyager 1* PLS model, this discrepancy is somewhat disturbing. A possible explanation, however, is the position

of *Galileo* with respect to the maximum in n_e . At such low T_i , the plasma is strongly confined and we do not yet fully understand where the plane of maximum density in the cold torus actually is (Schneider and Trauger 1995).

Quantitative models of the cold torus (Richardson and Siscoe 1983, Moreno and Barbosa 1986, Barbosa and Moreno 1988) were able to match (more or less) the conditions observed on the *Voyager 1* traversal of the cold torus (Bagenal 1985). However, the cold torus remains perplexing for several reasons. Firstly, it is unclear how the material reaches this region. The extended neutral clouds could be a source (Delamere *et al.* 2003a) although electron impact ionization will be extremely inefficient at cold torus electron temperatures (Brown *et al.* 1983a). Slow inward diffusion caused by persistent magnetospheric interchange motions driven by diurnal wind patterns in Jupiter's upper atmosphere (Brice and McDonough 1973) is an alternative candidate. Secondly, it is not understood why there should be a build-up of material at this distance from Jupiter. The density is clearly peaked at about 5.4 R_J in *Voyager* PLS and ground-based observations (Figure 23.9). Thirdly, it is completely unknown how this material can be ultimately removed and on what timescales this occurs. It is probable that ions in the cold torus are old but recombination at such cold temperatures has a timescale of the order of years.

The *Voyager 1* PLS measurements may have given two clues pointing towards the solution of these problems. First, a small but significant amount of SO_2^+ was seen in the cold torus (Figure 23.11). The SO_2 lifetime against photodissociation is only of the order of 1 hour at Jupiter's distance, whereas the timescale to transport sputtered material into this part of the torus is at least 10 times greater. Hence, although an SO_2 neutral cloud is present (Scherb and Smyth 1993) either a rapid transport mechanism is required or else some means of stabilising the molecule is needed (by the formation of a macromolecule, for example) until it reaches cold torus distances. The detection of high molecular weight molecules ($M/q > 500$ amu e^{-1}) has recently been reported (Frank and Paterson 2002).

The second clue is the presence in the same PLS spectrum (Figure 23.11) of a population of hot ions. It would be reasonable to infer that these are fresh pickup ions. Hence, there is probably a supply of neutrals (possibly through the dissociation and ionization of molecules) which are ionized and populate the cold torus. Charge exchange is almost certainly of some importance here also (Barbosa and Moreno 1988).

Given that ionizable material does appear to be drifting inwards towards Jupiter to produce the cold torus, it is interesting to ask where is the inner boundary of the torus (if such a boundary exists at all). The torus structure inside 5.0 R_J is, in reality, unknown. It is widely assumed that the density drops rapidly to near zero. However, this assumption is based upon *Voyager* PLS and *Galileo* observations (Bagenal *et al.* 1997, Frank and Paterson 2001b) at periapsis, which were not made in the centrifugal equator. Thus a plasma almost completely collapsed on to this plane may not have been detected. Brightness limits at optical wavelengths are difficult to define because of the contributions from emissions from the ribbon and outer torus along the line of sight. Emission may in any case be very weak because of low electron temperatures. If slow inward diffusion were

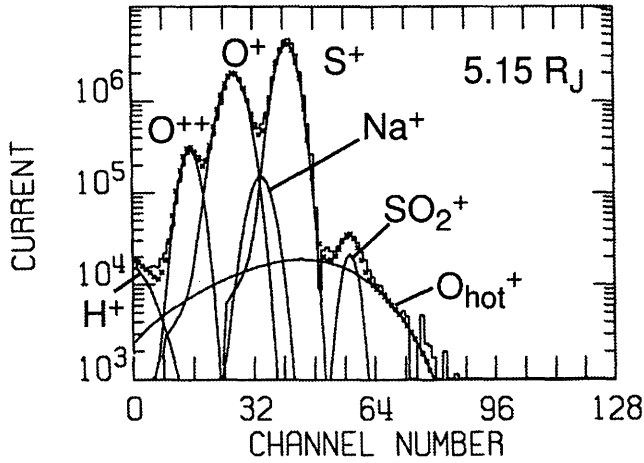


Figure 23.11. *Voyager 1* PLS spectrum acquired at 10:36 UT on March 6, 1979 when the spacecraft was 5.15 R_J from the planet. The spectrum shows a significant peak at energy channels 48–60 which was attributed to SO_2^+ and a small hot ion component (Bagenal 1985). The electron density is inferred to be 1260 cm^{-3} , $n(\text{SO}_2^+) \sim 0.25\%$, and $n(\text{hot}) \sim 2\%$.

to persist inwards of 5.0 R_J , a mechanism would still be required to remove the plasma. Absorption by macroscopic bodies may be a possibility but this, as with other mechanisms, is difficult to assess without detailed knowledge of the density distribution.

23.4.5 Longitudinal Structure

While described as temporal variations, changes in plasma parameters with System III longitude should really be thought of as spatial variations of the torus fixed in magnetic longitude as Jupiter rotates. Variations in S^+ emission intensity with Jupiter's rotation have been evident in torus data sets almost since observations first began (Trafton 1980). However, the most revealing work, which has linked intensity with temperature, is relatively recent.

It has been shown clearly (Schneider and Trauger 1995) that T_{\parallel} varies strongly with λ_{III} in the S^+ ribbon. A minimum, corresponding to about 25 eV was found near $\lambda_{\text{III}} = 200^\circ$ while the maximum (80 eV) was found near $\lambda_{\text{III}} = 80^\circ$ (Figure 23.12). It is significant that there is only one maximum in System III and that the maximum and minimum are not on exactly opposite sides of the torus.

It has been shown (Eq. 23.6 and 23.7) that, to first order, the density of plasma along a field line in the torus can be described by a scale height distribution. Thus, if the flux tube mass content in the flux tube through the ribbon were constant with System III, the density at the centrifugal equator would have to be lower in regions where the temperature is high. As intensity is proportional to n^2 , regions of high temperature should also have a lower peak brightness. Observations (Schneider and Trauger 1995) indicate that indeed the peak intensity and the temperature of the ribbon are anti-correlated, thereby explaining apparently contradictory results from simultaneous ground-based and *Ulysses* measurements – see Rauer *et al.* (1993), Desch *et al.* (1994), Schneider *et al.* (1997). Figure 23.12 (Schneider *et al.* 1997) shows that the flux-tube mass content in the ribbon does

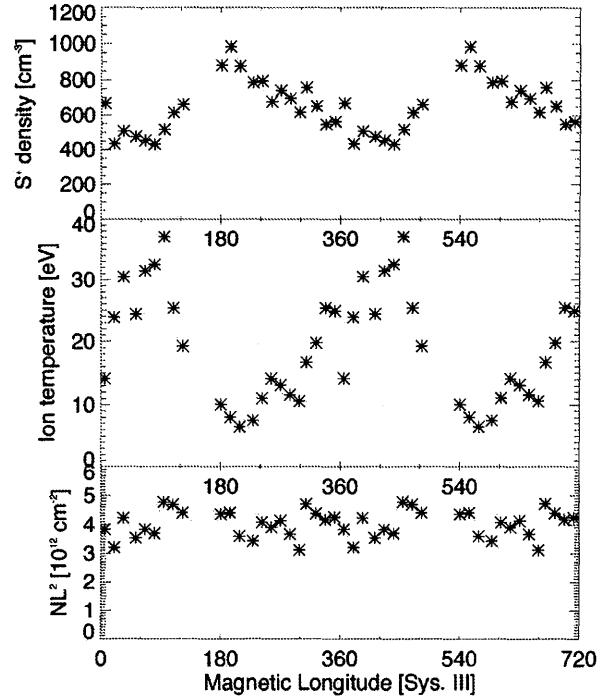


Figure 23.12. The variation in density, T_i , and flux tube content in the ribbon. Top: The brightness of the ribbon in S^+ converted to a density using the Colorado Io Torus Emission Package (Taylor *et al.* 1995). Middle: The derived ion temperature. Bottom: The flux tube content.

appear to be constant with System III assuming that S^+ is a proxy for all torus species in the ribbon (which, we repeat, is not necessarily the case).

Galileo PLS measurements during the C22 orbit (Frank and Paterson 2001b) do not, however, fit this picture. At $\lambda_{\text{III}} = 350^\circ$, the high T_i suggested by ground-based observations should lead to relatively high densities at large distances from the centrifugal equator. Frank and Paterson observed the opposite. At 0.7 R_J away from the symmetry plane, lower densities were observed at $\lambda_{\text{III}} = 350^\circ$ than at $\lambda_{\text{III}} = 216^\circ$. It must be noted, however, that *Galileo* was not in the ribbon for these observations which leads one to ask whether System III periodicities are restricted to the ribbon. Ground-based observations (M. Brown 1994, 1995) suggest that System III periodicities are present throughout the torus.

Searches for System III periodicities at other wavelengths have not proved so fruitful. In particular, the Extreme Ultraviolet Explorer (EUVE) data (Gladstone and Hall 1998, Lichtenberg 2000) have shown that at EUV wavelengths, there is little or no variation with System III. However, it is important to note that EUVE was a slitless spectrograph and that the period searches were carried out by integrating large volumes (both azimuthally and latitudinally) to derive their results. The anti-correlation of temperature and peak intensity implies that the size of the slit used to make period searches influences the result unless it is corrected for. A slit, tall in latitudinal extent, will integrate most of the emission and will show a much reduced amplitude when compared to a narrow slit centered on the centrifugal equator.

Herbert and Sandel (2000) have re-analysed *Voyager* UVS data from around the flyby and found small (12%) variations in n_e with anti-correlated variations in T_e . The slit in this case was smaller than for EUVE but it needs to be noted that the pointing of the spacecraft and instrument have considerable uncertainties. Thus, System III variations at EUV wavelengths cannot be excluded. Unambiguous identification of such a variation is, however, important. The ground-based observations suggest that more of the energy of the bulk electrons will be channeled into emission at $\lambda_{III} = 200^\circ$ than elsewhere and hence they will be cooler (Schneider *et al.* 1997). On the other hand, if at EUV wavelengths there is no System III asymmetry, it implies that the hot electrons forming the high energy tail of the distribution are being kept hot by an unknown mechanism.

The direct cause of the observed anti-correlation of temperature and peak intensity in S^+ emission remains unknown. The minimum of T_i in System III seems to coincide with the longitudes of some other phenomena in the jovian system. This region has been referred to as the “active sector” which is an empirical description attempting to relate several phenomena in the magnetosphere (Vasyliunas 1983, Hill *et al.* 1983).

23.4.6 Local-Time Symmetries

Material is finally removed from the system by outflow down the magnetotail. This loss process should lead to an electric field across the tail. Such a field was first postulated (Barbosa and Kivelson 1983, Ip and Goertz 1983) as an explanation of the local time asymmetry in the brightness of the torus seen in *Voyager* UVS data.

The electric field produced by the magnetotail flow effectively produces a shift in the corotation field acting roughly along the dawn–dusk line. The sense of the shift is such that ions on the dawn side of Jupiter are forced further away from the planet. This results in the plasma expanding. Its density drops and it cools. As radiation is proportional to the square of the density, the emission from the dawn ansa decreases. On the dusk ansa, the opposite occurs. The density rises, the plasma warms, and the emission increases. (It should be noted that seen from the Earth, this appears as an asymmetry between the east side and the west side of the torus leading to the effect frequently being referred to as an “east–west” asymmetry. As A. J. Dessler has pointed out, this is a misnomer.)

The observational evidence for this picture is now extremely strong. Morgan (1985) demonstrated the brightness asymmetry at optical wavelengths and showed that ratio of the convection field to the corotation field (ε) was around 0.04. The Extreme Ultraviolet Explorer data at 68.5 nm indicated a similar field strength (Hall *et al.* 1994, Thomas *et al.* 1996). The ribbon’s center of rotation (in addition to other motions) is shifted by about 0.3 R_J with respect to the OTD (Schneider and Trauger 1995). The temperature asymmetry has been illustrated by ground-based measurements of line broadening (Brown 1994b). It has even been possible to show that the spatial distribution of the neutral sodium banana cloud is affected by the dawn–dusk electric field in a quantifiable manner (Smyth and Combi 1988). The plasma density varies so strongly near Io’s orbit that a small spatial shift of the plasma with respect to Io produces a sig-

nificant change in the magnitude of the Na sink which, in turn, modifies the observed brightness distribution.

As the strength of the dawn–dusk electric field must be related to the mass of material flowing down the tail, one must assume that the magnitude of the field is related in some way to the total torus mass. Some evidence in support of this has been presented (Herbert and Hall 1998).

While this description fits most observational results, high time resolution observations of the ribbon at optical wavelengths appear to indicate that the situation is more complex. The ribbon position with respect to Jupiter, at the same System III longitude, shows small but measurable changes from one jovian rotation to the next (Schneider and Trauger 1995). The same authors also showed what appear to be aperiodic oscillations of the ribbon position on timescales less than System III. This is not at all understood. These oscillations may, however, be responsible for observed fluctuations in OI 630.0 nm emission from Io’s atmosphere (Oliverson *et al.* 2001).

23.5 COMPOSITION, RADIATION AND ENERGY LOSS

23.5.1 Collisional Excitation and Non-Maxwellian Distributions

Radiation allows us to probe torus characteristics remotely and is a major energy loss process. A total emission rate of 2.5×10^{12} W was estimated from UVS observations at the time of the *Voyager 1* flyby (Shemansky 1980). By the time *Voyager 2* arrived, the emission rate had doubled (Shemansky 1988). Subsequent revisions to the torus composition (particularly T_e) and to radiative cooling rates suggest lower emission rates at the *Voyager 1* encounter. There can, however, be little doubt that the total radiated power was of the order of 10^{12} W with a factor of 2 variation in time. A substantial part of this power is ultimately derived from ion pickup channelled through the electrons via Coulomb collisions (Spitzer 1962). The heated electrons excite ions which then lose this energy by emission of a photon. The detailed procedure for calculating emission rates (Osterbrock 1989) shows that

$$I \propto n_e n_i \quad (23.9)$$

where I is the emitted intensity and n_i is density of the emitting species. The collision strengths are strongly dependent upon T_e and require detailed atomic physics calculations. Tabulated values for species of importance have been presented by, for example, Tayal (1997) and Tayal and Gupta (1999). The CHIANTI database (Landi *et al.* 2002) is also a useful source of atomic data. The populations of electrons in each energy level of the ion require solution of a classical equilibrium problem. For the optical lines of S^+ , S^{2+} , O^+ , and O^{2+} , a five-level calculation is sufficient (see Brown *et al.* 1983a). However, the most important emissions for the energy budget are found in the EUV. The S^{2+} line at 68.0 nm has been estimated to account for 5% of the total radiative loss alone. An average radiated power of 1.7×10^{11} W from this line was observed with the Extreme Ultraviolet Explorer (Herbert and Hall 1998). Between 40.0 nm and 72.0 nm, the emitted power is typically 3.3×10^{11} W. Unfortunately, it is

at EUV wavelengths where errors in atomic physics parameters are greatest and hence extrapolation of observed EUV emission rates over the entire spectrum are prone to significant error. A possible method to reduce the uncertainty is to use the fact that S^{2+} , for example, has several lines in the EUV. As the excitation potential of the lines will be different, the line ratios can be used to constrain T_e and errors in atomic parameters (Herbert *et al.* 2001). However, this approach is not straightforward because the torus is known to have a non-Maxwellian electron distribution in the 3–50 eV energy range (Belcher 1983, Sittler and Strobel 1987, Meyer-Vernet *et al.* 1995, Frank and Paterson 2001b) and it is electrons in this energy range (not the “core” of the distribution) which are responsible for exciting EUV emissions. Knowledge of the tail of the electron distribution function is therefore critical. The suprathermal fraction also varies strongly with joventric distance (Belcher 1983).

It is possible to produce good fits to very high quality FUV spectra using a Maxwellian distribution (Feldman *et al.* 2001). However, it is clear that modeling using one Maxwellian will consistently require T_e values higher than the bulk temperature and may lead to distorted derived chemical compositions depending upon the wavelengths of lines used for the fit. Yet another complication which is not often considered is that collision strengths are generally provided integrated over a Maxwellian electron energy distribution, and it is not obvious that calculations using multiple Maxwellians to define the emission are entirely accurate.

The most complete spectra of the torus in the UV have been obtained by the UVIS experiment on *Cassini* (Esposito *et al.* 1998, Steffl *et al.* 2003). Figure 23.13 shows the *Cassini*/UVIS spectrum and identifies most of the observed lines. Attempts to model these spectra with multiple Maxwellians are currently ongoing.

Fortunately, at optical wavelengths, the tail of the distribution is completely insignificant and thus derivations of composition from remote sensing measurements in this wavelength range are likely to be relatively unaffected. There are four major difficulties, however.

First, the O^{2+} has only one weak optical line (at 500.7 nm) and S^{3+} has no optical lines. Thus, the high ionization states, which are important for investigating the electron distribution function (the ionization of S^{2+} to produce S^{3+} requires 35 eV electrons) are fairly poorly constrained. Secondly, the O^+ doublet at 372.7 and 372.9 nm is not an easy observation and the S^+ doublet at 406.9 and 407.6 nm, which is, in combination with the red S^+ lines, diagnostic of T_e does not, in reality, provide an adequate constraint. Thirdly, the 3-D structure of the torus implies that remote sensing experiments integrate torus properties along lines of sight. This can be particularly important for the ribbon and the cold torus. It can easily appear that there is a two-temperature component in the cold torus (e.g., Trauger 1984) when, in fact, the warm component is warm plasma from the outer torus along the line of sight. Careful modeling (Taylor *et al.* 1995, Herbert and Sandel 1995, Thomas 1996, Brown 1994b) is needed to extract the correct intensity at a specific joventric distance. Finally, there is time variability.

These complexities have led to considerable confusion in the past concerning the true composition of the torus. However, it is necessary to investigate this closely

because the composition and T_e determine the total radiative loss in a highly nonlinear way (Shemansky 1988, Smith *et al.* 1988). As we shall see, the present consensus is that the radiative losses from the torus lead to lower T_e values than can be accounted for by the energy input from pickup near Io. Thus, there must be an additional energy source.

23.5.2 Torus Composition

The major species in the torus are S^+ , S^{2+} , S^{3+} , O^+ , and O^{2+} but there are very few simultaneous measurements. Neither the in situ plasma detectors nor the UV spectrometers on *Voyager* and *Galileo* were able to separate all the species. The PLS experiments were not able to distinguish between S^{2+} and O^+ (they have the same mass/charge ratio) and the UVS experiments could not distinguish between O^+ and O^{2+} (the only bright emissions they have in the UVS range both occur at 83.3 nm). Earth-orbiting UV spectrometers (IUE, HST, HUT, FUSE and EUVE) either do not have sufficient spectral range to observe all major species and/or have poor spatial resolution. (As Figure 23.9 shows, spatial variations in torus properties occur over scales of 0.2 R_J and less.)

Our benchmark composition (Figure 23.2) is the result of a semi-empirical model based on PLS charge density, T_e , T_i , the analysis of UVS spectra between 5.75 and 8.25 R_J (Shemansky 1987), and PLS composition inside 5.75 and outside 8.25 R_J (Bagenal 1994). In the denser, warmer region between 5.7 and 7.5 R_J , the composition is fairly uniform. The densities of ions at higher ionization states (S^{3+} and O^{2+}) are low in the core of the torus ($\sim 2\%$) but increase with radial distance so that the average charge state, $\langle Z \rangle$, increases from 1.3 to 1.6 outside 8 R_J . Inside 5.7 R_J , where the density and temperature drop precipitously, the composition also changes abruptly. S^+ becomes the dominant ion and $\langle Z \rangle$ is close to unity. This overall picture has, in general, been supported by ground-based and Earth-orbiting observations. For example, detections of O^{2+} and S^{3+} in the optical and infrared, respectively, are consistent with this composition (Thomas 1993a, Lichtenberg *et al.* 2001).

Other observations and models of the composition show significant differences from the *Voyager* picture. Figure 23.14 illustrates these differences as determined from 12 observations and 5 neutral cloud theory (NCT) models (see below). The lower bar-chart shows the ratio of densities of sulfur ions ($S^+/S^{2+}/S^{3+}$) normalized to the density of S^{2+} . Since the errors in these densities are dominated by uncertainties in the underlying atomic data, showing the formal error bars from fits to the spectra would be rather misleading. The upper plot shows the average charge density, $\langle Z_i \rangle$ and the ratio of total oxygen ion densities to sulfur ion densities O/S. Unfortunately, there are no bright oxygen emissions in the FUV region so that the first 5 cases only involve the 3 sulfur ions.

A critical point to bear in mind here is that different measurement techniques can easily produce very different results. For example, the EUVE measurements of Hall *et al.* (1994) will be most sensitive to regions in the torus where T_e is relatively high. This is also where S^{2+} is more prevalent. Hence, although the EUVE measurements are a whole torus

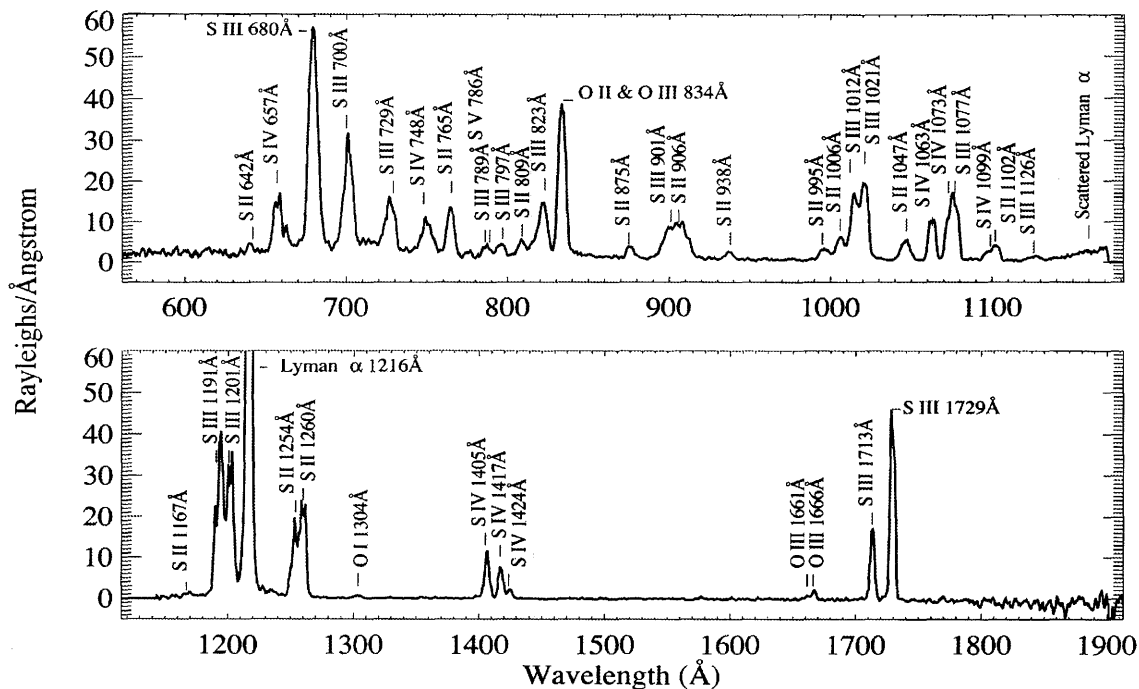


Figure 23.13. *Cassini* UVIS spectrum of the Io torus on January 14, 2001. The vertical axis represents the brightness of the torus integrated from 4 to 8 R_J radial distance and averaged over the latitudinal extent of the torus.

“average”, the composition derived will be biased towards higher ionization states than, say, visible spectroscopic data. Similarly, with EUVE, the dawn–dusk asymmetry produces a T_e asymmetry which, in turn, can affect the derived torus mass and composition. Having said this, EUVE results have an advantage over optical techniques because EUVE detected the emission lines with the highest power loss from the torus.

Although we have referred exclusively to EUVE in the above paragraph, every measurement technique has advantages and disadvantages. Knowing this, groups have sought to make simultaneous observations with different experiments to remove the influence of time variability but this has so far met with limited success.

Looking in detail at Figure 23.14, the average charge state is remarkably steady, varying only between 1.3 and 1.5. (In the first 5 cases the dominant ion O^+ is missing which probably results in an exaggerated average charge state.) The O/S ratio varies wildly between 0.5 and 3. If this reflects a true temporal variation (rather than poor measurement of the oxygen ion density) then the implication is that the nature of the source changes, perhaps reflecting a change in the relative contributions of S_2 vs. SO_2 . Regarding the sulfur ions, the amount of S^+ seems the most variable, perhaps reflecting changes in T_e . S^{3+} seems to have higher abundance in observations made at wavelengths sensitive to electrons at higher energies (e.g., EUVE). But it is difficult to resolve this issue until the emission rates and the electron distribution function are known reliably.

In addition to the major species, a number of minor species have been detected in the torus including Na^+ (Hall *et al.* 1994), Cl^+ and Cl^{2+} (Küppers and Schneider 2000, Feldman *et al.* 2001), C^{2+} (Feldman *et al.* 2004) and S^{4+} (Steffl *et al.* 2003). Other minor species are likely to be

present reflecting the composition of Io’s atmosphere, surface, and interior (transported to the atmosphere and surface via volcanic activity). The only species which is likely to be present in sufficient numbers to affect substantially the energetics of the torus is H^+ which may be either iogenic or from Jupiter. It is often assumed that 10% of torus ions are H^+ . However, while proton densities in the jovian plasmasheet and cold inner torus are well determined by in situ measurements (Belcher 1983), they are difficult to separate from high densities of heavy ions in the Io plasma torus. Frank and Paterson (1999) reported a proton density of 60 cm^{-3} measured by the PLS instrument on *Galileo* in the immediate vicinity of Io. They argued that half of these protons are local pickup protons, in which case they would be highly anisotropic ($T_{\perp} \gg T_{\parallel}$) and confined to the equator. Chust *et al.* (1999) inferred a lower limit for the H^+ density of 0.5% (10 cm^{-3} for total torus density of 2000 cm^{-3}) from *Galileo* plasma wave data near Io. Tighter constraints on the proton density at high latitudes (where protons dominate the composition) are provided by studies of wave propagation. Estimates of the proton density from modeling the dispersion of whistler waves (propagating from Jupiter to the torus) have steadily decreased from early estimates of 15–20% of the total flux tube content (Tokar *et al.* 1982), to the Crary *et al.* (1996) estimate of 5% (maximum density = 50 cm^{-3}), and, most recently, to a proton density of 3–8 cm^{-3} estimated by Wang *et al.* (1998a,b) at high latitudes for torus L -shells. This constraint is consistent with limits placed on the total electron density at high latitudes from observed Faraday rotation of jovian radio emission reported by Melrose and Dulk (1991). Finally, we note that Zarka *et al.* (2001) estimated the proton concentration to be 1–3% of the torus density ($20\text{--}60\text{ cm}^{-3}$) in the Io wake region, based on the minimum frequency of Io-dependent decametric radio emission.

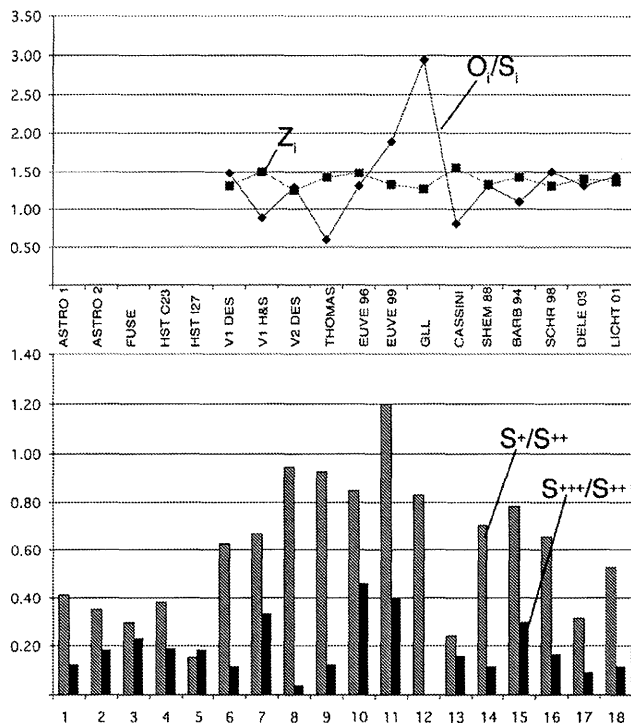


Figure 23.14. Composition variability: The top panel illustrates variability of average charge state (Z_i) and total ion abundance ratio (O_i/S_i), and the bottom panel shows sulfur mixing ratios for the following 17 observations and NCT models 1–3, HUT and FUSE (Feldman *et al.* 2001); 4–5, HST (Herbert *et al.* 2002); 6, Ion composition from analysis of *Voyager 1* UVS spectra by D. E. Shemansky (Bagenal 1994); 7, Analysis of *Voyager 1* UVS spectra (Herbert 2000); 8, *Voyager 2* UVS (Shemansky 1987); 9, Ground-based spectroscopic observations taken in 1999 (Thomas *et al.* 2001); 10–11, EUVE data (Herbert and Hall 2001); 12, *Galileo* PLS data obtained Dec. 1996 (Crary *et al.* 1998); 13, *Cassini* UVIS data from Jan. 2000 (Steffl *et al.* 2003); 14, NCT model of Shemansky (1988); 15, NCT model ($O/S = 3$) of Barbosa *et al.* (1994); 16, NCT model of Schreier *et al.* (1998); 17, NCT model of this paper; 18, NCT model of Lichtenberg (2001). (From Delamere and Bagenal 2003.)

23.6 NEUTRAL CLOUD THEORY (NCT)

Since neutral oxygen and sulfur species from Io seem to be the main source for the torus, the next step is to see if NCT models of production and loss processes can match the observed plasma conditions (Barbosa *et al.* 1983, Shemansky and Smith 1981, Smith and Strobel 1985, Shemansky 1988, Barbosa 1994, Schreier *et al.* 1998, Lichtenberg 2000, Delamere and Bagenal 2003). While these models only involve ionization products of sulfur and oxygen, they entail on the order of 25 significant reactions and 35 major emission lines. Further complications come from uncertainties and variations in the underlying atomic data (e.g., Strobel 1989, Herbert *et al.* 2001). In this section, results are presented using the Delamere and Bagenal 1-dimensional (box) model (cf. Shemansky 1988) which uses the current best estimates of atomic data.

Figure 23.15 shows the flows of mass and energy through a “typical”, *Voyager*-like torus and is consistent

with earlier models of *Voyager 1* conditions (Delamere and Bagenal 2003). It should be noted that modeling the conditions prevalent during the *Voyager 2* and *Cassini* flybys require rather different inputs.

The input sources to such models are sulfur and oxygen atoms (either as a fixed neutral density or as a neutral source rate). The observed composition requires that the ratio of oxygen to sulfur neutral sources be greater than 2 (which would result from dissociation of pure SO_2 , for example). This arises because of the efficiency of the $\text{O} + \text{O}^+ \rightarrow \text{O}^+ + \text{O}^*$ charge-exchange reaction which removes oxygen neutrals preferentially.

A total source rate of $10 \times 10^{-4} \text{ cm}^{-3} \text{ s}^{-1}$ is consistent with net plasma production of $1.4 \times 10^{28} \text{ ions s}^{-1}$ or 560 kg s^{-1} for a source volume of $1.4 \times 10^{31} \text{ cm}^3$ and a mean molecular weight of 24. Note that dividing a typical local electron density of 2000 cm^{-3} by the total source strength of $10 \times 10^{-4} \text{ cm}^{-3} \text{ s}^{-1}$, one obtains a timescale for replenishment of the torus of ~ 20 days. Equivalently, in a 10-hour jovian rotation period, only $\sim 2\%$ of the torus is replenished.

The neutral clouds of S and O are also ionized by electron impact ionization. Sulfur is ionized about 5 times faster than oxygen by this process. Major problems in the construction of NCT models arise from changes in published values for the ionization rate coefficients for different ions as a function of T_e , particularly at lower energies. The addition of small quantities of suprathermal electrons enhances the ionization rate by $\sim 30\%$, particularly to higher ionization states. When ionized, the fresh ion picks up gyromotion at the local flow speed (see Section 23.3). The ionization of neutral S and O supplies only $\sim 20\%$ of total power input.

Charge-exchange reactions between ions do not change the total charge density, but they have major effects on composition as well as providing (through pickup of fresh ions) $\sim 65\%$ of the power to the torus.

Radial transport of plasma out of the torus is usually simplified in NCT models to a loss timescale $\tau \sim 8$ to 80 days, though most (*Voyager*-era) models are converging on a lifetime of 40–60 days. The radial transport of plasma is a relatively minor loss of mass (33%) and, particularly, energy (carrying away only 10% of the torus power).

The energy picked up by a fresh ion is transferred by Coulomb collisions to electrons (at a rate of $0.17 \text{ eV cm}^{-3} \text{ s}^{-1}$). The ion cooling timescale is ~ 20 days (i.e., comparable to the transport timescale). The electrons quickly lose energy through excitation of the ions (which promptly radiate the energy, mostly at EUV wavelengths). The EUV emissions radiated by the torus add up to about $0.28 \text{ eV cm}^{-3} \text{ s}^{-1}$ which is about 70% of the total torus power throughput.

To produce this power it was pointed out by Shemansky (1988) and Smith *et al.* (1988) that pickup energy is not sufficient. The problem arises because the transfer of energy from ions to electrons (via Coulomb collisions) is not efficient enough. The electrons therefore cool to temperatures which are insufficient to produce the observed ion partitioning and radiative output. The electrons require an additional energy source. Several authors have investigated the efficacy of different potential sources of energy (Smith *et al.* 1988, Barbosa 1994, Schreier *et al.* 1998) but there is a growing consensus that a small fraction of suprathermal electrons can readily supply the necessary additional 18% of the total power. The most efficient coupling would occur should the

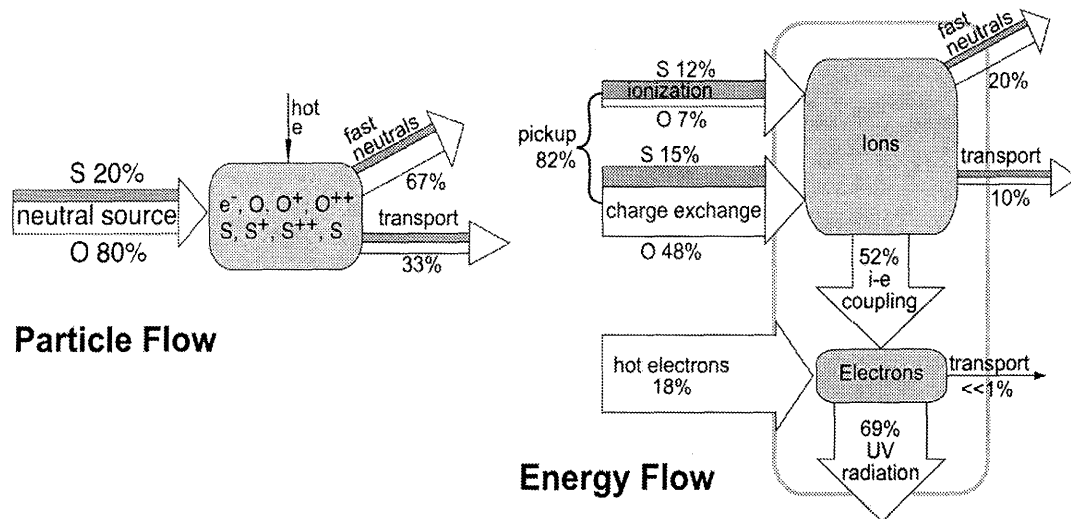


Figure 23.15. The flow of particles and energy through the Io plasma torus from a neutral cloud theory model for *Voyager 1* conditions. The total particle flow is $10^{-3} \text{ cm}^{-3} \text{ s}^{-1}$ and the total energy flow is $0.4 \text{ eV cm}^{-3} \text{ s}^{-1}$. (From Delamere and Bagenal 2003.)

suprathermal electrons have a temperature about 5 times that of the thermal electrons (i.e., about 20–30 eV) (Schreier *et al.* 1998). *Voyager* in situ electron measurements indicate a small (1–2%) fraction of ~ 500 eV electrons (Sittler and Strobel 1987). In models of the torus, the temperature and charge fraction of the hot electrons can be varied to adjust the total power output (sensitive to electrons in the 5–30 eV range for EUV emissions) and to match observed fractions of ionization states. It needs to be noted, however, that there is no clear consensus on where the suprathermal electrons get their energy. Acceleration by waves (Barbosa 1994), coupling to the observed high energy electron beams (Williams *et al.* 1996), or generation in interchange events (Frank and Paterson 2000a) appear to be plausible mechanisms.

Figure 23.15 shows the mass and energy flow with the following 5 input parameters: diffusion time $\tau = 50$ days, neutral source $S = 10^{-3} \text{ cm}^{-3} \text{ s}^{-1}$, oxygen/sulfur ratio of the neutral source ($S_{\text{O}}/S_{\text{S}} = 4$), hot electron temperature $T_{\text{eh}} = 600$ eV, hot electron fraction $F_{\text{eh}} = 0.23\%$. Starting with a basically empty torus, the model comes to equilibrium with $n_e = 2000 \text{ cm}^{-3}$ and $T_e \sim 4$ eV. The ions settle into different temperatures, cooler for higher ionization states because of the faster coupling to electrons for ions with more charge ($T(\text{S}^+) = 100$ eV, $T(\text{S}^{2+}) = 75$ eV, $T(\text{S}^{3+}) = 40$ eV, $T(\text{O}^+) = 90$ eV and $T(\text{O}^{2+}) = 60$ eV). Hence, it is not expected that T_i should be the same for all species (see Thomas *et al.* 2001).

Figure 23.15 shows that, in the main source region of the torus (5.9–6.5 R_J), 1/3 of the mass and $<10\%$ of the energy is removed by transport. Thus, conditions are controlled by local production, charge exchange and radiation. Farther out in the torus, where the neutral cloud density has dropped, we expect reactions to slow down and the transport rate to increase. Local plasma conditions are then increasingly dependent on what is transported into the region. Models (Schreier *et al.* 1998) of the evolution of plasma conditions using NCT and radial diffusion seem to match the *Voyager* radial profiles of plasma conditions quite well.

It should be noted that the Delamere and Bagenal

model, as with many others published to date, does not include the effect of the non-homogeneity of the neutral source around the torus, the latitudinal distribution, or the inhomogeneous nature of the ionization sink. It is also restricted to one dimension.

23.7 OUTWARD PLASMA TRANSPORT

As the torus is in a quasi-steady state, the net mass input at Io must be balanced by mass loss. While calculations and estimates cited above suggest that around 2/3 of the mass that leaves Io is lost via charge exchange, for the plasma itself, this is a mass neutral process. Several processes can contribute to mass loss in a minor way (e.g., recombination and “sweeping-up” by Europa) but the only effective loss process for the remaining 1/3 of the mass input is expansion into the middle magnetosphere and eventual loss into interplanetary space.

Oxygen and sulfur ions have been detected well away from the optically visible part of the torus by several spacecraft, e.g., *Voyager* (Belcher 1983), *Ulysses* (Geiss *et al.* 1992), and *Galileo* (Frank and Paterson 2001b). Flux-tube interchange has been suggested as a mechanism for transporting this material and recent *Galileo* observations have been interpreted in these terms (Thorne *et al.* 1997, Bolton *et al.* 1997, Kivelson *et al.* 1997, Frank and Paterson 2000a). We now discuss these processes in more detail.

Because the plasma is magnetically trapped, transport away from the source implies either inward or outward radial transport across magnetic L -shells. And because Jupiter’s magnetosphere is a giant centrifuge, outward transport is energetically favored over inward transport by a very wide margin. Indeed, centrifugally-driven outward transport is an automatic consequence of the radially-confined plasma source that Io imposes on Jupiter’s rotation-dominated magnetosphere. The theoretical problem turns out to be, not explaining why outward transport occurs, but explaining why

it occurs so slowly. Or, put another way, why is the torus so long-lived, and therefore so massive?

When the torus was discovered, it was immediately recognized that it was unstable to centrifugally-driven interchange motions (Richardson and Siscoe 1981, Siscoe and Summers 1981). The interchange instability is the magnetospheric analog of the Rayleigh-Taylor instability, the same instability that drives convection in a planetary atmosphere or a pot of boiling water. The effective gravity, dominated by the centrifugal force of corotation, is radially outward, and the mass source is located deep in the inner magnetosphere, where it would presumably be surrounded by a relative vacuum in the absence of outward transport. The essence of the centrifugally-driven interchange instability is that heavily-loaded magnetic flux tubes from the source region move outward by $\mathbf{E} \times \mathbf{B}$ drift and are replaced by inward-moving flux tubes containing less mass, thereby reducing the (centrifugal) potential energy of the overall mass distribution without significantly altering the configuration of the confining magnetic field. The interchange rate is regulated by Jupiter's conductivity and probably by other factors described below; in the absence of any regulating factor it would proceed at Jupiter's spin rate Ω (Hill 1986).

The centrifugal interchange instability can be analyzed theoretically either in terms of an MHD energy principle for fully-developed turbulence (e.g., Siscoe and Summers 1981, Southwood and Kivelson 1987) or in terms of a linear eigenmode analysis of plasma drift waves (e.g., Huang and Hill 1991). The two formalisms give basically the same answer: the predicted timescale for outward transport is

$$\tau \sim \frac{\Sigma B_E^2}{n_o m_i H \Omega^2 \beta} \sim (3\text{hr}) \frac{\Sigma}{1S} \quad (23.10)$$

where Σ is the effective Pedersen conductance of Jupiter's ionosphere (in units of [Siemens]), $B_e \approx 2\mu T$ is Jupiter's magnetic field strength at Io's orbit, $n_o \approx 2000 \text{ cm}^{-3}$ is the equatorial ion number density at the peak of its radial distribution, $m_i \approx 24 \text{ amu}$ is the mean ion mass, $H \approx 1 \text{ R}_J$ is the vertical scale height of the ion density distribution about the centrifugal equator, $\Omega \approx 2\pi/(10 \text{ hr})$ is the rotation rate of Jupiter, and

$$\beta \equiv -\frac{d \log(\eta)}{d \log(L)} \sim 2 \quad (23.11)$$

is a dimensionless parameter measuring the steepness of the inward gradient of flux-tube content η outside its peak near $L = 6$. (A value $\beta = 2.2$ was obtained by Bagenal (1989) from analysis of *Voyager 1* PLS observations.) The flux-tube content

$$\eta \equiv \int \frac{n ds}{B} \sim \frac{2n_o H}{B_e} \quad (23.12)$$

would be conserved along streamlines in the absence of sources and sinks. All of the parameters in Eq. 23.10. are accurately known except for Σ , which is still subject to at least an order-of-magnitude uncertainty. Aeronomical calculations assuming only solar photoionization (Strobel and Atreya 1983) set a lower limit of $\Sigma > \sim 0.2S$; auroral precipitation could increase this by perhaps an order of magnitude, but probably not by two orders of magnitude. Thus, a straightforward application of standard theory gives a transport timescale of nominally 3 hr, and probably no more than

30 hr. However, as noted in Sections 23.1 and 23.6, global empirical arguments seem to require a mean residence time $> \sim 8 \text{ days} \approx 200 \text{ hr}$. This discrepancy is too large to sweep under the rug.

Something other than Jupiter's ionospheric conductance (included in Eq. 23.10) is evidently regulating the outward transport of iogenic plasma. Two possibilities have been proposed. One is the "ring current impoundment" mechanism (Siscoe *et al.* 1981, Summers and Siscoe 1985a, Summers *et al.* 1988, Huang and Hill 1991), where the inward gradient of torus centrifugal potential energy content (essentially proportional to η) is almost balanced by an outward gradient of thermal energy content of the surrounding "ring current" plasma that is hotter but less dense than torus plasma (and ultimately derived therefrom). In terms of the MHD energy principle (Summers and Siscoe 1985a), the impoundment process can be summarized by the statement that the centrifugal potential energy liberated by outflow of cold torus plasma is expended not only in Joule heating of Jupiter's ionosphere (at a rate proportional to Σ) but also in compression of the ring-current plasma that must flow inward to compensate (i.e., to conserve magnetic flux). In terms of the drift-wave analysis (Huang and Hill 1991), the same process can be summarized by the statement that the divergence of the centrifugal drift current of cold torus plasma is almost balanced by an opposite divergence of the gradient/curvature drift current of the surrounding ring-current plasma. (The two drift currents are in the same (eastward) direction but their divergences are of opposite sign because the flux-tube contents of the two populations have opposing radial gradients.) The two approaches again give essentially the same answer.

It has proved difficult to assess the ring-current impoundment mechanism empirically because it depends on a delicate balance between two radial profiles, neither of which is very well constrained observationally. For example, an important fraction of the ring-current particles fall in the energy gap ($\sim 6\text{--}30 \text{ keV}$) that was not measured by the *Voyager* spacecraft. The torus ions, although more fully measured in energy space, are subject to uncertainty in deducing flux-tube content from local density measurements in the presence of non-Maxwellian velocity distributions, as described above. The most detailed empirical study of this question (Mauk *et al.* 1996) concludes that the energy content of ring-current ions is not sufficient to impede significantly the outward transport of torus plasma by the ring-current impoundment mechanism, although uncertainties remain. From a theoretical point of view, it can be argued that the mechanism runs afoul of Ockham's Razor in that it requires an additional population of plasma in just the right place, with just the right radial profile of energy content, to impede the loss of torus plasma. A radial gradient in the right direction (outward) is guaranteed by the fact that the ring-current particles have a source in the outer magnetosphere and a sink near Io's orbit, where they are lost by precipitation into Jupiter's atmosphere or replaced by lower-energy particles through charge exchange (e.g., Thorne 1983). But the magnitude of the gradient must also be just about right, and there is no obvious mechanism for maintaining such a delicate balance.

A second mechanism for impeding outward transport has been proposed (Pontius *et al.* 1998) which is referred

to as “velocity shear impoundment”. This mechanism relies only on the velocity shear of the observed corotation lag of torus plasma as described above (a peak with height $\sim 0.05 \Omega$ and radial width $\sim 1 R_J$). The peak magnitude of the velocity shear is $\chi = r|d\omega/dr| \sim \Omega/4$, or about 1/2 the growth rate $\gamma = 1/\tau \sim \Omega/2$ obtained from Eq. 23.10 with $\Sigma = 1S$. On the basis of an analytical model of linear perturbations and numerical simulations of their nonlinear development, Pontius *et al.* (1998) conclude that this observed shear rate is sufficient to arrest any perturbation whose initial amplitude is much less than the radial width of the velocity trough. The velocity shear does not merely slow the growth of the perturbations, it stops it, giving an asymptotic ($t \rightarrow \infty$) amplitude that is a finite multiple

$$\frac{A(\infty)}{A_0} = \exp\left(\frac{\pi\gamma}{2\chi}\right) \quad (23.13)$$

of the initial amplitude A_0 . The effect is illustrated in Figure 23.16 (a quantitative plot of the analytic solution developed by Pontius *et al.* 1998). The x and y directions correspond to radially outward from Jupiter, and the corotation direction, respectively. The shaded region is bounded by two isocontours of η (decreasing to the right), which are initially perturbed by a small sine wave (initial amplitude/wavelength = $\exp(-\pi/4)/2\pi \approx 0.07$). When the velocity shear $\chi = 0$ (top row), the perturbation grows exponentially at the rate γ (the time labels are in units of $\tau = 1/\gamma$). For a plausible shear rate $\chi = \gamma$ (bottom row), the amplitude approaches an asymptotic value $\exp(\pi/2) \approx 4.8$ times its initial value. The numerical simulations show the same qualitative behavior. It is interesting to note that, if the initial perturbation has amplitude $A_0 \sim R_{Io}$, and if $\chi \approx \gamma/2$ (the nominal value), then the asymptotic amplitude is $A(\infty) \sim 20 R_{Io} \sim 0.5 R_J$, comparable to the radial thickness of the torus. The velocity-shear effect is thus a plausible mechanism for restraining the outward transport of torus plasma to a rate that is compatible with the inferred residence time. The much stronger velocity shear that is likely to exist at the edges of Io’s corotational wake may likewise explain the radial confinement of newly-injected plasma within a ribbon-like structure (Goldstein *et al.* 2001). Note in Figure 23.8 that the ribbon is inward of the region of maximum deviation from corotation and therefore possibly confined by the corresponding velocity shear.

Although the timescale for outward transport of torus plasma is reasonably well constrained by observations, the spatial structure of the convection cells is not. The linear drift-wave theory (e.g., Huang and Hill 1991) cannot address this question because the convection cells are necessarily nonlinear. Early models of the nonlinear consequences of the centrifugal interchange instability (e.g., Siscoe and Summers 1981, Summers and Siscoe 1985a) were based on the assumption of fully developed turbulence, i.e., small circular eddies were assumed to form, disappear, and reform at random locations on a timescale comparable to their circulation frequency. This assumption was motivated by mathematical convenience, not by empirical or theoretical considerations. Numerical simulations of the centrifugal interchange instability utilizing the RCM-J (Rice Convection Model – Jupiter) code (Yang *et al.* 1992, 1994, Pontius *et al.* 1998, Goldstein *et al.* 2001) suggested that its nonlinear development takes the form of radially-aligned “fingers” of out-

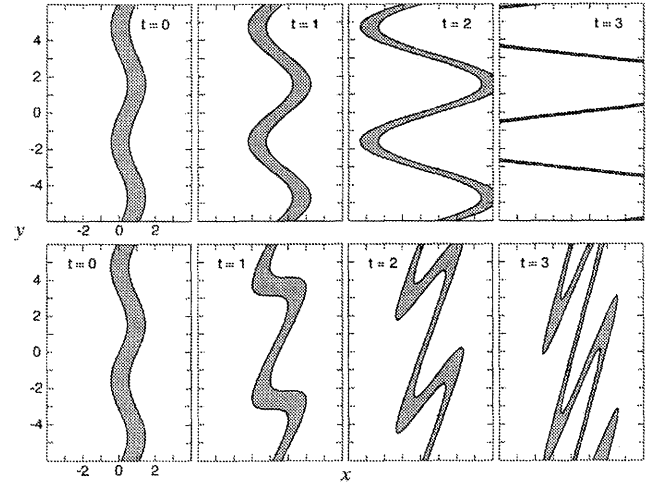


Figure 23.16. Quantitative plot of the analytical model discussed by Pontius *et al.* (1998), illustrating the effect of a background velocity shear on the development of the centrifugal interchange instability. With no shear (top row), a small perturbation of the torus density structure grows exponentially at the rate γ (the time unit is $\tau = 1/\gamma \sim 3 \text{ hr}(\Sigma/1S)$ from Eq. 23.10). With a realistic background shear $\chi = \gamma$ (bottom row), the perturbation grows only to a finite multiple around 5 times its initial amplitude.

flowing torus plasma interspersed with inflowing channels of more tenuous plasma from the outside. The dominant “wavelength” (finger spacing) is comparable to the length scale of the background gradient $\partial\eta/\partial r$, or $LR_J/\beta \sim 3R_J$ where β is defined in Eq. 23.11 above. However, it was found (Pontius *et al.* 1998) that when the background corotation lag is included in the simulations, the fingers become sheared in the azimuthal direction, which has two effects: it reduces the radial transport rate as described above, and it also deflects the radial flow channels into azimuthal ones, thus producing new radial fine structure. This behavior is already evident in the lower-right panel of Figure 23.16, and the fine structure itself is unstable to correspondingly smaller-scale perturbations. Moreover, there is another, smaller natural length scale of the system, the scale $\sim R_{Io}$ of the Io–torus interaction which produces large perturbations of the flow field if not of η itself. Recent RCM-J simulations resolving this smaller scale size (Goldstein *et al.* 2001) suggest that the Io–torus interaction drives the plasma density (and flow) structure to ever-decreasing scale sizes which are ultimately limited by the S^+ gyroradius ($\sim 20 \text{ km} \sim 0.01 R_{Io}$) if nothing else. The result may be a homogenization of the torus that conceals the underlying fine structure. This is significant because empirical studies have attempted, and failed, to find dramatic density structure ($> \sim 10\%$) down to scale sizes $< \sim R_{Io}$ utilizing both in situ (Richardson and McNutt 1987) and remote (Küppers and Schneider 1998) observations.

The radial transport rate is likely to vary systematically with System III longitude. For example, the minimum transport timescale (Eq. 23.10) is proportional to Σ/η and, although η is found to be remarkably uniform in longitude (Schneider and Trauger 1995), Σ is almost certainly not, owing to the extreme asymmetry of Jupiter’s near-surface

magnetic field. Thus, the conclusion that radial transport is dominated by small-scale structures does not preclude large-scale System III asymmetries in the magnetosphere resulting from asymmetric outward transport of torus plasma. This is the basic hypothesis of the magnetic anomaly/corotation convection model (e.g., Dessler and Vasyliunas 1979, Vasyliunas and Dessler 1981), although the transport process is now recognized to be much more complex than the global two-cell convection pattern depicted in early descriptions of the corotating convection model (e.g., Hill *et al.* 1981).

23.8 VARIABILITY IN TORUS EMISSIONS

23.8.1 Long-Term Variability

Although it was not immediately clear at the time, ground-based observations in the late 1970s were already indicating that the torus is a time variable phenomenon. Direct optical imaging using CCDs finally took away arguments that differences in measured intensities were related to different positions of slits with respect to the maximum emission. These observations showed that on timescales of a year or so, the S^+ 673.1 nm emission could vary by a factor of 4 (Jockers *et al.* 1992). Other observers have also demonstrated that the ribbon, while frequently by far the most prominent feature, could almost disappear at times (Jockers *et al.* 1992). It has been established that this is not related to short-term variabilities (such as System III and “System IV”) (N. M. Schneider, personal communication).

Following the long-term evolution of the torus requires huge amounts of observing because changes do not appear to be abrupt but gradual. Continuous access to Earth-orbiting and ground-based telescopes tends to be limited to, by comparison, relatively short periods. However, the *Cassini* ultraviolet imaging spectrometer experiment (UVIS) was able to take a long series of observations prior to the flyby of Jupiter in December 2000. The results were remarkable in that they showed a gradual transition from a torus where the sulfur ionization state was dominated by S^+ and S^{2+} to one dominated by S^{2+} and S^{3+} (Figure 23.17). The S^{3+} emission at 65.9 nm rose steadily through the observing period while the S^+ emission at 90.7 nm decreased.

The increase in the mean ionization state must result from an increase in T_e and/or the suprathermal tail of the electron energy distribution. As the electrons lose energy through radiation and the radiative rate is proportional to $n_e n_i$, the increased T_e must be related to a decrease in torus density. The drop in total emitted power further suggests reduction in the supply rate. At the time of writing, the UVIS data have not been completely analysed so that density estimates are not yet available. However, Herbert and Hall (1998) have also tried to establish this link between density and temperature using EUVE data. Using data acquired between 1993 and 1995, around the time of the Comet D/Shoemaker-Levy 9 impact with Jupiter*, they showed

that T_e and n_e were anti-correlated while the total luminosity at EUV wavelengths remained relatively stable. Here too, compositional differences were evident. While the estimated n_e rose by around 50%, the total EUV luminosity rose by only 24% as T_e dropped. However, in this case, there was no unambiguous correlated change in the ionization state but a rise in the O^+/S^+ mixing ratio.

So what provokes the change in density and temperature? It has generally been assumed that this must be related to the source, Io. We have seen in Section 23.6 that in NCT models, an increase in source rate leads to an increase in n_e and lower T_e . In Section 23.2, we also noted that ground-based observations of Na emission show that most, if not all, loss mechanisms have a high degree of time variability. Occasionally, direct pickup from Io’s ionosphere appears to be a strong process, at other times it does not. Similarly, while the loss from Io of molecular ions is sometimes present, often it is not. Thus, the source is variable, although because we are using sodium as a tracer, it is not clear to what extent. Models suggest a fairly simple relationship between source strength and torus properties (Section 23.6). However, establishing the direct link observationally is difficult because of the timescales involved and the fact that the major neutrals near Io (SO_2 , SO, S, and O) are extremely hard to observe. We also remain fairly ignorant of the details of the interaction between Io and the impinging magnetosphere and how these details are influenced by changing torus density and temperature. For example, if sputtering is the main mechanism by which material is removed from Io, increased plasma density results in increased sputtering and a positive feedback loop occurs. Some means of stabilizing the system would then be needed (see review Schneider *et al.* 1991).

The evidence for torus supply mechanisms other than sputtering breaks one feedback loop but the problem is not solved—merely more complicated. If direct pickup from Io’s ionosphere is a major supply mechanism, one would expect it to be influenced by the flow of plasma about Io and the Birkeland current system linking Io to Jupiter’s ionosphere. If the torus density were to increase, it is not clear how the supply rate would respond, if at all.

It has been shown that in regions of lower neutral and ion densities (where charge exchange is less important) radial transport becomes the major loss mechanism for the torus itself. It seems likely that an increase in torus supply leads directly to increased loss by this mechanism. This seems to be supported by the only attempt to study the link between supply and torus properties (Brown and Bouchez 1997). The Na cloud and the S^+ torus brightnesses were observed over a number of weeks. The observed timescales and magnitudes of changes were then used to constrain the stabilizing process. Based on Huang and Siscoe (1986), it has been shown that at the time of a sharp (> factor of

several months. Herbert and Hall found this “provocative” but not convincing. It is trivial to demonstrate that the comet could have easily supplied this amount of mass if only about 10^{-6} of its mass were picked-up by the torus. However, (1) the comet’s composition was probably dominated by carbon, water, nitrogen, and silicates and not by sulfur, (2) most of the mass was not charged and therefore could not be picked-up and (3) given the residence time of plasma in the torus, it is difficult to explain the persistence of the phenomenon over several months.

* Observations originally appeared to show that the D/Shoemaker-Levy 9 impacts had no measurable effect on the torus (Brown *et al.* 1995 and Hall *et al.* 1995). On detailed analysis of EUVE data, Herbert and Hall (1998) reported a 20% jump in n_e and corresponding decrease in T_e . This persisted for

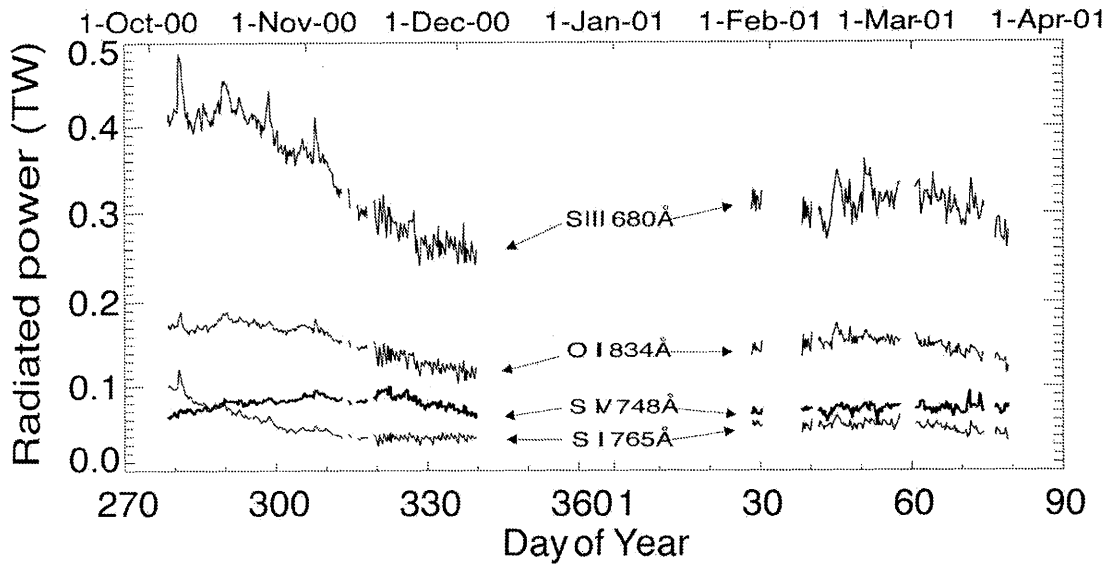


Figure 23.17. Total power radiated from the brightest spectral feature of the four major ion species present in the Io torus based on *Cassini* UVIS observations (Steffl *et al.* 2003). The data have been smoothed by taking the 3-hour running average around each observation. Over a period of 50 days the S^{3+}/S^{2+} emission ratio almost doubled while the S^+/S^{2+} ratio decreased by about 50%. The emitted power in the strongest EUV line (S^{2+} at 68.0 nm) almost halved over this period.

3) increase in Na brightness, the S^+ torus initially reduced in mass before rising rapidly (Brown and Bouchez 1997). It was concluded that a nonlinear increase in loss from the torus balanced increased neutral supply. On the other hand, in order to accept that an increasing Io source modified the torus in this case, one still has to assume that Na is a tracer for S and that S^+ is a tracer for total torus mass.

23.8.2 Comparisons of *Voyager* and *Galileo* Results

The in situ measurements by the *Galileo* PLS and by the *Galileo* plasma wave spectrometer (*Galileo* PWS) offer the chance to make direct comparisons between data acquired during multiple passages by the orbiter and our “benchmark” model of the torus from *Voyager 1* measurements. Instead of providing refinements to the model, however, the new data have provided as many questions as answers. For example, there remain discrepancies of more than 50% between the *Galileo* PWS and *Galileo* PLS determinations of electron density for which at present there are no clear explanations (cf. Frank and Paterson 2001b, Gurnett *et al.* 2001). When we examine the *Galileo* PLS observations of plasma density and temperature we see significant variations from orbit to orbit (Figs. 23.18, 23.19 and 23.20) but it is difficult to distinguish if variations are temporal or spatial.

Figure 23.18 shows the trajectories of *Galileo* through the torus. The trajectories are identified by the orbit number (e.g., C23 where C indicates that a close approach to Callisto was made on that orbit) and are superimposed upon the 2-D electron density distribution derived from *Voyager* observations by Bagenal (1994).

Figs. 23.19 and 23.20, show the ratios of the *Galileo* PLS n_e and T_{\perp} determinations to those predicted by the benchmark and orders the data by radial distance in the torus and by System III longitude.

There are several noteworthy points. Firstly, the *Galileo* observations of T_{\perp} are within about 30% of the *Voyager*-based model values. *Galileo* values tend to be lower in the region between 6 and 7 R_J and perhaps higher at greater joviocentric distances. Inside 6 R_J the ratio is scattered. The plot of temperature *vs.* System III longitude suggest some systematic behavior (higher temperatures at longer longitudes) but the I24 data (squares) are a strong exception. This may be in part because of temporal variability, fine structure (inside Io’s orbit) and/or the effect of the dawn-dusk asymmetry.

Secondly, n_e is highly variable and there is no clear trend in the difference between *Voyager* and *Galileo*. This is particularly surprising in the region between 6 and 7 R_J where deviations from the model are up to a factor of 3. (Note that the ion density from *Galileo* PLS has been multiplied by 1.5 in this plot in order to make the comparison with the *Voyager*-based model which gives electron density.)

Thirdly, density measurements inside 6 R_J give a range of deviations from the model of over one order of magnitude. The deviations for the JOI passage almost cover this full range, for example. Only some of this can be attributed to the passage of the spacecraft near Io. When we look at the plot of density organized by System III longitude we see that for a single trajectory (e.g., C23 shown with diamonds) there seems to be a systematic variation with longitude. But the C23 peak at 180° longitude is not reflected in data from other orbits.

A separate approach to temporal variability is taken by Frank and Paterson (2001a,b) who looked at occasions when the *Galileo* spacecraft passed through similar locations in radial distance and System III longitude. They found that the first orbit (J0) had much higher density than the C22 and C23 orbits at the same location, the torus at C23 was denser than at I24, while C21, C22 and I25 seem to have similar densities. All of the temperatures were similar ($6-8 \times 10^5$ K)

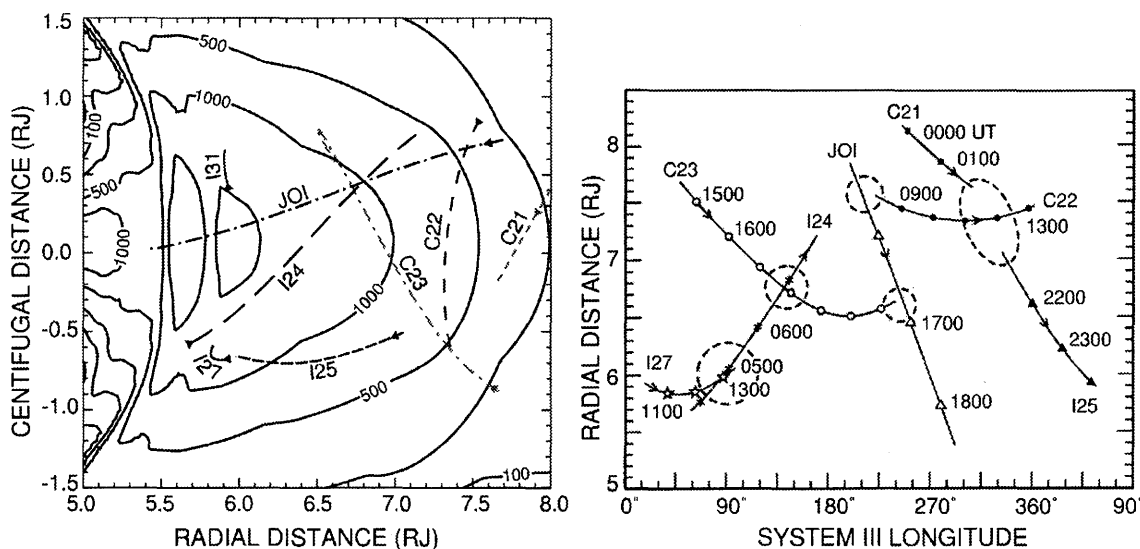


Figure 23.18. The trajectories of several passes of the *Galileo* spacecraft through the Io plasma torus. The pass number is a compound of the orbit number and the satellite targeted on that orbit. (E.g., C23 = 23rd orbit with Callisto as the target moon for the orbit). Density contours (left) are from Bagenal (1994). The right figure is adapted from Frank and Paterson (2001b), W. Paterson, personal communication).

except for the distant C21 orbit (7.5–8 R_J) where the temperature was 13×10^5 K. While the multiple traversals of the torus by the *Galileo* spacecraft have shown us significant similarities and differences in the torus properties from orbit to orbit, they point to the fact that unique separation of temporal and spatial variations requires either multiple spacecraft (as demonstrated in the Earth's magnetosphere) or monitoring with remote sensing.

23.8.3 “System IV”

While analysing a series of observations of the torus at 953.1 nm, Roesler *et al.* (1982) noticed that their S^{2+} intensity data appeared almost random when ordered by System III longitude. On the other hand, when they re-ordered the data according to a period 3% longer than System III, a near-perfect sinusoidal oscillation was evident. Narrow-band kilometric (nKOM) emissions and *Voyager* UVS measurements showed similar properties which led to the proposal of a new periodicity in Jupiter's magnetosphere which was referred to as System IV (Sandel and Dessler 1988).

The most detailed study of this phenomenon has been made by M. Brown (1995). His observations over a period of more than 6 months clearly indicated a periodicity of around 2.91% longer than System III. It had previously been thought this was the result of deviations from corotation, but Brown was able to show that while the region where corotation deviation was evident was restricted to near Io's orbit (see above), the “System IV effect” was clearly seen over a much wider range of radial distances. Furthermore, Brown reported a phase shift of 180° in the brightness oscillation mid-way through his 6-month observation run (see also Woodward *et al.* 1997). These observations effectively rule out any link to corotation deviation and supported previous theoretical arguments against such a link (Dessler 1985).

EUVE observations have again been used to search for

similar periodicities in the EUV but no evidence for any System IV periodicity has so far been found (Lichtenberg 2000, Gladstone and Hall 1998). As with System III, this may be the result of poor spatial and temporal resolution and low signal to noise.

There can be little doubt that periodicities in the torus around 3% longer than System III are present. However, it is by no means clear that the periods are stable. Woodward *et al.* (2000), for example, have observed different periods (cf. Brown 1994b, Roesler *et al.* 1982) although again fairly close to 3%. The differences in results and Brown's phase shift are evidence against System IV being a beat frequency between Io's orbital period and System III. Tests for spurious periods by Brown also suggest that System IV is a real phenomenon.

It has been proposed that System IV is related to long-lived density waves (Brown 1994b). Their periods may then be related to the sound speed in the plasma which, in turn, is density dependent. Thus, knowing the strong fluctuations in torus density, one would not expect the System IV period to be constant. A key observation is therefore to relate observed System IV periods to torus mass.

23.8.4 Short Timescale Variations

Shorter timescale variations (shorter than 10 hr) have also been claimed for the torus. In particular, Volwerk *et al.* (1997) have observed that the dawn and dusk ribbon emissions are uncorrelated with a 5-hr time lag from one to the other, implying time variations on 5-hr timescales.

Glassmeier *et al.* (1989) have also suggested the presence of eigenoscillations of the whole magnetosphere with periodicities on the order of 10 to 20 minutes. They suggest that the torus should show “breathing modes” (expansions and contractions) which would change the position of the plasma with respect to the jovian rotation axis and modulate the observed brightness.

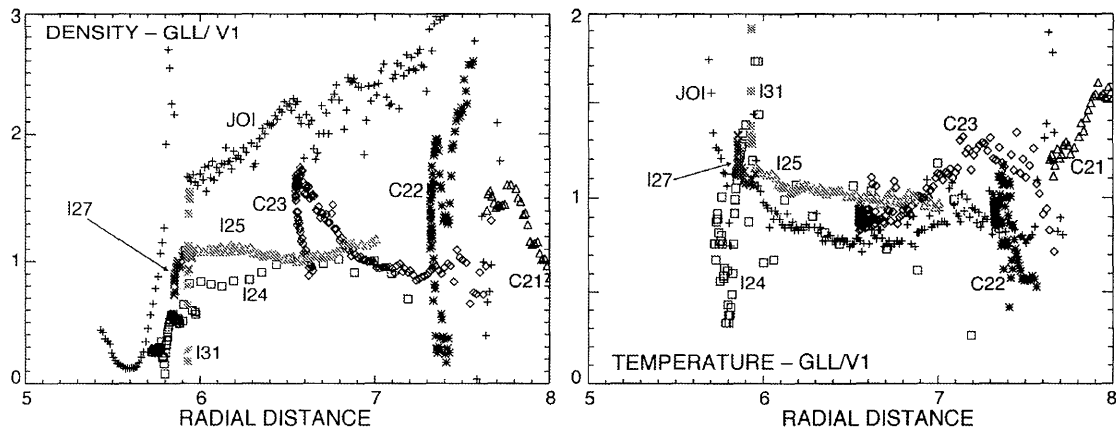


Figure 23.19. For the trajectories in Figure 23.18, the ratio of the observed (left) electron density and (right) ion temperature to that predicted by the *Voyager*-based model of Bagenal (1994) and ordered by radial distance. The *Galileo* data were measured by PLS (Frank and Paterson 2001b, W. Paterson, personal communication).

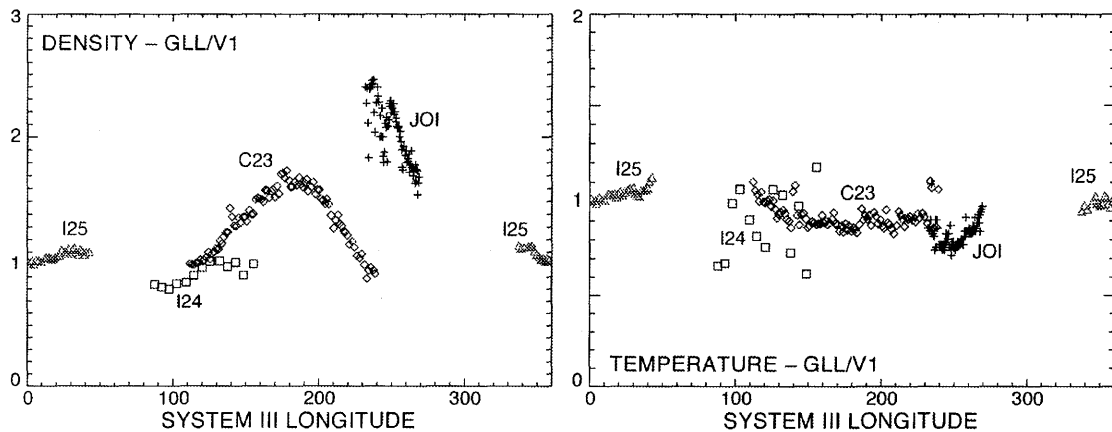


Figure 23.20. For the trajectories in Figure 23.18, the ratio of the observed (left) electron density and (right) ion temperature to that predicted by the *Voyager*-based model of Bagenal (1994) and ordered by System III longitude. Only data acquired between 6 and 7 R_J has been used in order to remove effects associated with the complex structure seen near Io's orbit. The *Galileo* data were measured by PLS (Frank and Paterson 2001b, W. Paterson, personal communication).

23.9 OUTSTANDING QUESTIONS

Much of the physics describing the input, transport, and loss of torus material is relatively poorly known and hence it is quite straightforward to construct a long list of detailed questions which still need to be answered. On the other hand, there are a few fundamental issues about which we have working hypotheses but they remain nonetheless unproven.

1. Is the immediate region about Io the dominant source of mass and energy or are the neutral clouds remote from Io more important? The model of Smyth and Marconi suggests that the ribbon can be produced by an essentially local source (although some of this will also come from the remote cloud). Recent modeling of the neutral cloud distributions by these authors also suggest a highly local source. The observed broad spread of the deviation from corotation does not require an extended source because of Io's relative motion with respect to the jovian magnetic field. On the other hand, estimates based on the interaction between Jupiter's magnetosphere and Io indicate that less than 20% of the

energy can be supplied locally (Bagenal 1997, Saur *et al.* 2003).

2. Is the high energy tail of the electron distribution function sufficient to balance the observed radiative losses and, if so, how is it maintained? The existence of a high energy tail is fairly well established but its form and energy content are not.

3. Flux-tube interchange is becoming accepted as the means by which material is transported into the middle magnetosphere but the spatial structure and temporal development of the interchange process have not been established, either observationally or theoretically.

4. What produces the observed variability in System III? At present, there is no consensus on the cause of this behavior (although there are simple models). The minimum in ion temperature roughly coincides with the maximum jovian surface magnetic field strength. Further clues to the origin of the System III effect may be provided by the fact that the ribbon is systematically offset from its expected equilibrium latitude.

5. What processes are acting to heat the plasma beyond about $7 R_J$? Expansion and radiation should continue to cool the plasma but this is offset by other processes.

6. How do changes in Io's volcanic activity and/or its atmosphere affect the torus? The link between long-term variability in the torus and Io's volcanic atmosphere has not yet been made (although Brown and Bouchez (1997) have made an excellent start in this direction observationally, and Johnson and McGrath (1993) theoretically). The key here lies in the details of the atmospheric structure and the interaction, both of which are themselves complex and, in some ways, not well understood.

It is apparent that the production, maintenance and loss processes in the Io plasma torus will remain the subjects of complex and intriguing research for many years to come.

Acknowledgments. The authors would like to thank the following people for providing data (sometimes ahead of publication) and for useful discussions: A. J. Dessler, R. E. Johnson, N. M. Schneider, P. Feldman, W. Paterson, A. I. F. Stewart, L. Esposito, K. Khurana, N. Krupp, A. Steffl, P. Delamere. FB acknowledges support from NASA grants NAG5-7088 and through JPL 959550. TWH acknowledges support from NASA grants NAG5-6432 and NAG5-8131. The first drafts of this chapter were made when NT was at the Max-Planck-Institut für Aeronomie.

REFERENCES

- Ansher, J. A., W. S. Kurth, D. A. Gurnett, and C. K. Goertz, High resolution measurements of density structures in the jovian plasma sheet, *Geophys. Res. Lett.* **19**, 2281–2284, 1992.
- Badnell, N. R., Dielectronic recombination rate coefficients for $S^{(q+)}$ ($q = 1-5$) ions, *Astrophys. J.* **379**, 356–358, 1991.
- Bagenal, F., Plasma conditions inside Io's orbit: *Voyager* measurements, *J. Geophys. Res.* **90**, 311–324, 1985.
- Bagenal, F., Torus-magnetosphere coupling, in *Time Variable Phenomena in the Jovian System*, M. J. S. Belton, R. A. West, and J. Rahe, eds, pp. 196–210, NASA SP-494, 1989.
- Bagenal, F., Empirical model of the Io plasma torus: *Voyager* measurements, *J. Geophys. Res.* **99**, 11 043–11 062, 1994.
- Bagenal, F., Ionization source near Io from *Galileo* wake data, *Geophys. Res. Lett.* **24**, 2111–, 1997.
- Bagenal, F. and J. D. Sullivan, Direct plasma measurements in the Io torus and inner magnetosphere of Jupiter, *J. Geophys. Res.* **86**, 8447–8466, 1981.
- Bagenal, F., F. J. Crary, A. I. F. Stewart, N. M. Schneider, D. A. Gurnett, W. S. Kurth, L. A. Frank, and W. R. Paterson, *Galileo* measurements of plasma density in the Io torus, *Geophys. Res. Lett.* **24**, 2119–, 1997.
- Barbosa, D. D., Neutral cloud theory of the jovian nebula: Anomalous ionization effect of superthermal electrons, *Astrophys. J.* **430**, 376–386, 1994.
- Barbosa, D. D. and M. G. Kivelson, Dawn-dusk electric field asymmetry of the Io plasma torus, *Geophys. Res. Lett.* **10**, 210–213, 1983.
- Barbosa, D. D. and M. A. Moreno, A comprehensive model of ion diffusion and charge exchange in the cold Io torus, *J. Geophys. Res.* **93**, 823–836, 1988.
- Barbosa, D. D., F. V. Coroniti, and A. Eviatar, Coulomb thermal properties and stability of the Io plasma torus, *Astrophys. J.* **274**, 429–442, 1983.
- Belcher, J. W., Physics of the jovian magnetosphere, in *The Low-Energy Plasma in the Jovian Magnetosphere*, pp. 68–105, A. J. Dessler (ed.), Cambridge University Press, 1983.
- Belcher, J. W., The Jupiter-Io connection: An Alfvén engine in space, *Science* **238**, 170–176, 1987.
- Bolton, S. J., R. M. Thorne, D. A. Gurnett, W. S. Kurth, and D. J. Williams, Enhanced whistler-mode emissions: Signatures of interchange motion in the Io torus, *Geophys. Res. Lett.* **24**, 2123–2126, 1997.
- Brice, N. M. and T. R. McDonough, Jupiter's radiation belts, *Icarus* **18**, 206–219, 1973.
- Brown, M. E., Observation of mass loading in the Io plasma torus, *Geophys. Res. Lett.* **21**, 847–850, 1994a.
- Brown, M. E., Observations of mass loading in the Io plasma torus, *Geophys. Res. Lett.* **21**, 847–850, 1994b.
- Brown, M. E., *The Structure and Variability of the Io Plasma Torus*, Ph.D. thesis, University of California, Berkeley, 1994a.
- Brown, M. E., Periodicities in the Io plasma torus, *J. Geophys. Res.* **100**, 21 683–21 696, 1995.
- Brown, M. E. and A. H. Bouchez, The response of Jupiter's magnetosphere to an outburst on Io, *Science* **278**, 268–271, 1997.
- Brown, M. E. and R. E. Hill, Discovery of an extended sodium atmosphere around Europa, *Nature* **380**, 229–231, 1996.
- Brown, M. E., E. J. Moyer, A. H. Bouchez, and H. Spinrad, Comet Shoemaker-Levy 9: No effect on the Io plasma torus, *Geophys. Res. Lett.* **22**, 1833–1836, 1995.
- Brown, R. A., Optical line emission from Io, in *Exploration of the Planetary System*, R. A. Brown, ed., pp. 527–531, Reidel, 1974.
- Brown, R. A., The Jupiter hot plasma torus: Observed electron temperature and energy flows, *Astrophys. J.* **244**, 1072–1080, 1981.
- Brown, R. A., The probability distributions of S^+ gyrospeeds in the Io torus, *J. Geophys. Res.* **87**, 230–234, 1982.
- Brown, R. A., Observed departure of the Io plasma torus from rigid corotation with Jupiter, *Astrophys. J.* **268**, L47–L50, 1983.
- Brown, R. A. and N. M. Schneider, Sodium remote from Io, *Icarus* **48**, 519–535, 1981.
- Brown, R. A. and Y. L. Yung, Io, its atmosphere and optical emissions, in *Jupiter*, T. Gehrels (ed), University of Arizona Press, pp. 1102–1145, 1976.
- Brown, R. A., C. B. Pilcher, and D. F. Strobel, Spectrophotometric studies of the Io torus, in *Physics of the Jovian Magnetosphere*, A. J. Dessler (ed.), Cambridge University Press, pp. 197–225, 1983a.
- Brown, R. A., D. E. Shemansky, and R. E. Johnson, A deficiency of O III in the Io plasma torus, *Astrophys. J.* **264**, 309–323, 1983b.
- Burger, M. H., N. M. Schneider, and J. K. Wilson, *Galileo*'s close-up view of the Io sodium jet, *Geophys. Res. Lett.* **26**, 3333–3336, 1999.
- Carlson, R. W. and D. L. Judge, *Pioneer 10* ultraviolet photometer observations of the jovian hydrogen torus: The angular distribution, *Icarus* **1975**, 395–399, 1975.
- Chamberlain, J. and D. M. Hunten, *Theory of Planetary Atmospheres*, McGraw-Hill, 2nd ed., 1987.
- Chust, T., A. Roux, S. Perraut, P. Louarn, W. S. Kurth, and D. A. Gurnett, *Galileo* plasma wave observations of iogenic hydrogen, *Planet. Space Sci.* **47**, 1377–1387, 1999.
- Clarke, J. T., G. Ballester, J. Trauger, J. Ajello, W. Pryor, K. Tobiska, J. E. P. Connerney, G. R. Gladstone, J. H. Waite, L. B. Jaffel, and J. Gérard, Hubble Space Telescope imaging of Jupiter's UV aurora during the *Galileo* orbiter mission, *J. Geophys. Res.* **103**, 20 217–20 236, 1998.
- Cloutier, P. A., R. E. Daniell, A. J. Dessler, and T. W. Hill, A cometary ionosphere model for Io, *Astrophys. Space Sci.* **55**, 93–112, 1978.

- Combi, M. R., K. Kabin, T. I. Gombosi, D. L. Dezeew, and K. G. Powell, Io's plasma environment during the *Galileo* flyby: Global three-dimensional MHD modeling with adaptive mesh refinement, *J. Geophys. Res.* **103**, 9071–9082, 1998.
- Connerney, J. E. P., Magnetic fields of the outer planets, *J. Geophys. Res.* **98**, 18,659, 1993.
- Connerney, J. E. P., M. H. Acuña, N. F. Ness, and T. Satoh, New models of Jupiter's magnetic field constrained by the Io flux tube footprint, *J. Geophys. Res.* **103**, 11 929–11 940, 1998.
- Crary, F. J., F. Bagenal, J. A. Ansher, D. A. Gurnett, and W. S. Kurth, Anisotropy and proton density in the Io plasma torus derived from whistler wave dispersion, *J. Geophys. Res.* **101**, 2699–2706, 1996.
- Crary, F. J., F. Bagenal, L. A. Fran, and W. R. Paterson, *Galileo* plasma spectrometer measurements of composition and temperature in the Io plasma torus, *J. Geophys. Res.* **103**, 29 359, 1998.
- Cremonese, G., F. Marzari, N. Eccli, and G. Corrain, The Io sodium cloud: Comparison between observations and numerical models, *Icarus* **131**, 138–151, 2000.
- Cummings, W. D., A. J. Dessler, and T. W. Hill, Latitudinal oscillations of plasma within the Io torus, *J. Geophys. Res.* **85**, 2108–2114, 1980.
- Delamere, P. A. and F. Bagenal, Modeling variability of plasma conditions in the Io torus, *J. Geophys. Res.* **108**, 1276, 2003.
- Delamere, P. A., F. Bagenal, R. Ergun, and Y.-J. Su, Momentum transfer between the Io plasma wake and Jupiter's ionosphere, *J. Geophys. Res.* **108**, 1241, 2003a.
- Delamere, P. A., F. Bagenal, R. E. Ergun, and Y.-J. Su, Momentum transfer between the Io plasma wake and Jupiter's ionosphere, *J. Geophys. Res.* **108**, 1276, 2003b.
- Desch, M. D., W. M. Farrell, and M. L. Kaiser, Asymmetries in the Io plasma torus, *J. Geophys. Res.* **99**, 17 205, 1994.
- Dessler, A. J., Coordinate systems, in *Physics of the Jovian Magnetosphere*, A. J. Dessler (ed.), Cambridge University Press, pp. 498–504, 1983.
- Dessler, A. J., Differential rotation of the magnetic fields of gaseous planets, *Geophys. Res. Lett.* **12**, 299–302, 1985.
- Dessler, A. J. and V. M. Vasyliunas, The magnetic anomaly model of the jovian magnetosphere: Predictions for *Voyager*, *Geophys. Res. Lett.* **6**, 37–40, 1979.
- Durrance, S. T., P. D. Feldman, and H. A. Weaver, Rocket detection of ultraviolet emission from neutral oxygen and sulfur in the Io torus, *Astrophys. J.* **267**, L125–L129, 1983.
- Durrance, S. T., P. D. Feldman, W. P. Blair, A. F. Davidsen, G. A. Kriss, J. W. Krukv, K. S. Long, and H. W. Moos, Neutral sulfur emission from the Io torus measured with the Hopkins Ultraviolet Telescope, *Astrophys. J.* **447**, 408–415, 1995.
- Esposito, L. W., J. E. Colwell, and W. E. McClintock, *Cassini* UVIS observations of saturn's rings, *Planet. Space Sci.* **46**, 1221–1235, 1998.
- Eviatar, A., Y. Mekler, and F. V. Coroniti, Jovian sodium plasma, *Astrophys. J.* **205**, 622–633, 1976.
- Feldman, P. D., T. B. Ake, A. F. Berman, H. W. Moos, D. J. Sahnou, D. F. Strobel, H. A. Weaver, and P. R. Young, Detection of chlorine ions in the Far Ultraviolet Spectroscopic Explorer spectrum of the Io plasma torus, *Astrophys. J.* **554**, L123–L126, 2001.
- Frank, L. A. and W. R. Paterson, Intense electron beams observed at Io with the *Galileo* spacecraft, *J. Geophys. Res.* **104**, 28 657–28 699, 1999.
- Frank, L. A. and W. R. Paterson, Production of hydrogen ions at Io, *J. Geophys. Res.* **104**, 10 345–10 354, 1999.
- Frank, L. A. and W. R. Paterson, Observations of plasmas in the Io torus with the *Galileo* spacecraft, *J. Geophys. Res.* **105**, 16 017–16 034, 2000a.
- Frank, L. A. and W. R. Paterson, Return to Io by the *Galileo* spacecraft: Plasma observations, *J. Geophys. Res.* **105**, 25 363–25 378, 2000b.
- Frank, L. A. and W. R. Paterson, Passage through io's ionospheric plasmas by the *Galileo* spacecraft, *J. Geophys. Res.* **106**, 26 209–26 224, 2001a.
- Frank, L. A. and W. R. Paterson, Survey of thermal ions in the Io plasma torus with the *Galileo* spacecraft, *J. Geophys. Res.* **106**, 6131–6150, 2001b.
- Frank, L. A. and W. R. Paterson, Plasmas observed with the *Galileo* spacecraft during its flyby over Io's northern polar region, in *Journal of Geophysical Research (Space Physics)*, Volume 107, Issue A8, pp. SMP 31-1, CiteID 1220, DOI 10.1029/2002JA009240, pp. 31–1, 2002.
- Frank, L. A., W. R. Paterson, K. L. Ackerson, V. M. Vasyliunas, F. V. Coroniti, and S. J. Bolton, Plasma observations at Io with the *Galileo* spacecraft, *Science* **274**, 394–395, 1996.
- Geiss, J., G. Gloeckler, H. Balsiger, L. A. Fisk, A. B. Galvin, F. Gliem, D. C. Hamilton, F. M. Ipavich, S. Livi, and U. Mall, Plasma composition in Jupiter's magnetosphere: Initial results from the Solar Wind Ion Composition Spectrometer, *Science* **257**, 1535–1539, 1992.
- Gladstone, G. R. and D. T. Hall, Recent results from EUVE observations of the Io plasma torus and Jupiter, *J. Geophys. Res.* **103**, 19 927–19 934, 1998.
- Glassmeier, K.-H., N. F. Ness, M. H. Acuna, and F. M. Neubauer, Standing hydromagnetic waves in the Io plasma torus: *Voyager 1* observations, *J. Geophys. Res.* **94**, 15 063–15 076, 1989.
- Goertz, C. K., Io's interaction with the plasma torus, *J. Geophys. Res.* **85**, 2949–2956, 1980.
- Goldberg, B. A., G. W. Garneau, and S. K. LaVoie, Io's sodium cloud, *Science* **226**, 512–516, 1984.
- Goldreich, P. and D. Lynden-Bell, Io, a jovian unipolar inductor, *Astrophys. J.* **156**, 59–78, 1969.
- Goldstein, J. W., T. W. Hill, R. W. Spiro, and R. A. Wolf, Fine structure of the Io plasma torus produced by the centrifugal interchange instability, in *Jupiter Conference*, Boulder, June 2001, 2001.
- Gurnett, D. A., A. M. Persoon, W. S. Kurth, A. Roux, and S. J. Bolton, Electron densities near Io from *Galileo* plasma wave observations, *J. Geophys. Res.* **106**, 26 225–26 232, 2001.
- Haff, P. K., C. C. Watson, and Y. L. Yung, Sputter ejection of matter from Io, *J. Geophys. Res.* **86**, 6933–6983, 1981.
- Hall, D. T., G. R. Gladstone, H. W. Moos, F. Bagenal, J. T. Clarke, P. D. Feldman, M. A. McGrath, N. M. Schneider, D. E. Shemansky, D. F. Strobel, and J. H. Waite, Extreme Ultraviolet Explorer satellite observation of Jupiter's Io plasma torus, *Astrophys. J.* **426**, L51–L54, 1994.
- Hall, D. T., G. R. Gladstone, F. Herbert, R. Lieu, and N. Thomas, Io torus EUV emissions during the Comet Shoemaker–Levy/9 impacts, *Geophys. Res. Lett.* **22**, 3441, 1995.
- Herbert, F., A simple transport model for the Io plasma torus “ribbon”, *Geophys. Res. Lett.* **23**, 2875, 1996.
- Herbert, F. and D. T. Hall, Disentangling electron temperature and density in the Io plasma torus, *J. Geophys. Res.* **103**, 19 915–19 926, 1998.
- Herbert, F. and B. R. Sandel, Radial profiles of ion density and parallel temperature in the Io plasma torus during the *Voyager 1* encounter, *J. Geophys. Res.* **100**, 19 513–19 530, 1995.
- Herbert, F. and B. R. Sandel, Azimuthal variation of ion density and electron temperature in the Io plasma torus, *J. Geophys. Res.* **105**, 16 035–16 052, 2000.
- Herbert, F., G. R. Gladstone, and G. E. Ballester, Extreme Ultraviolet Explorer spectra of the Io plasma torus: Improved spectral resolution and new results, *J. Geophys. Res.* **106**, 26 293–26 310, 2001.

- Hill, T. W., Inertial limit on corotation, *J. Geophys. Res.* **84**, 6554–6558, 1979.
- Hill, T. W., Corotation lag in Jupiter's magnetosphere: Comparison of observation and theory, *Science* **207**, 301–302, 1980.
- Hill, T. W., Convection in planetary magnetospheres, in *Comparative Study of Magnetospheric Systems*, pp. 201–215, 1986.
- Hill, T. W. and F. C. Michel, Heavy ions from the Galilean satellites and the centrifugal distortion of the jovian magnetosphere, *J. Geophys. Res.* **81**, 4561–4565, 1976.
- Hill, T. W. and D. H. Pontius, Plasma injection near Io, *J. Geophys. Res.* **103**, 19 879–19 886, 1998.
- Hill, T. W. and D. H. Vasyliunas, Jovian auroral signature of Io's corotational wake, *J. Geophys. Res.* **107**, 27–1, 2002.
- Hill, T. W., A. J. Dessler, and F. C. Michel, Configuration of the jovian magnetosphere, *Geophys. Res. Lett.* **1**, 3–6, 1974.
- Hill, T. W., A. J. Dessler, and L. J. Maher, Corotating magnetospheric convection, *J. Geophys. Res.* **86**, 9020–9028, 1981.
- Hill, T. W., A. J. Dessler, and C. K. Goertz, Magnetospheric models, in *Physics of the Jovian Magnetosphere*, A. J. Desler (ed.), Cambridge University Press, pp. 353–394, 1983.
- Huang, T. S. and T. W. Hill, Drift wave instability in the Io plasma torus, *J. Geophys. Res.* **96**, 14 075, 1991.
- Huang, T. S. and G. L. Siscoe, Stability of the Io torus, *J. Geophys. Res.* **91**, 10 163–10 166, 1986.
- Ip, W.-H. and C. K. Goertz, An interpretation of the dawn–dusk asymmetry of UV emission from the Io plasma torus, *Nature* **302**, 232–234, 1983.
- Jockers, K., N. Thomas, T. Bonev, V. Ivanova, and V. Shkodrov, Observations of Io's sodium cloud and torus, *Adv. Space Res.* **12**, 347–351, 1992.
- Johnson, R. and M. McGrath, Stability of the Io plasma torus/atmosphere interaction, *Geophys. Res. Lett.* **20**, 1735–1738, 1993.
- Johnson, R. E., Plasma ion heating of an SO₂ atmosphere on Io, *Geophys. Res. Lett.* **16**, 1117–1120, 1989.
- Johnson, R. E., Formation of Na-containing molecular ions at Io, *Icarus* **111**, 65–72, 1994a.
- Johnson, R. E., Plasma-induced sputtering of an atmosphere, *Space Sci. Rev.* **69**, 215–253, 1994b.
- Kivelson, M. G., K. K. Khurana, R. J. Walker, J. A. Linker, C. T. Russell, D. J. Southwood, and C. Polansky, A magnetic signature at Io: Initial report from the *Galileo* magnetometer, *Science* **273**, 337–340, 1996a.
- Kivelson, M. G., K. K. Khurana, R. J. Walker, J. Warnecke, C. T. Russell, J. A. Linker, D. J. Southwood, and C. Polansky, Io's interaction with the plasma torus: *Galileo* magnetometer report, *Science* **274**, 396–398, 1996b.
- Kivelson, M. G., K. K. Khurana, C. T. Russell, and R. J. Walker, Intermittent short-duration magnetic field anomalies in the Io torus: Evidence for plasma interchange?, *Geophys. Res. Lett.* **24**, 2127, 1997.
- Kivelson, M. G., K. K. Khurana, R. Lopes, and E. Turtle, Polar passes by Io: Limits on the internal field and sources of field-aligned currents in the polar cap, in *Eos*, 2002.
- Krimigis, S. M. and colleagues, A nebula of gases from Io surrounding Jupiter, *Nature* **415**, 994–996, 2002.
- Kumar, S., The SO₂ atmosphere and ionosphere of Io: Ion chemistry, atmospheric escape, and models corresponding to the *Pioneer 10* radio occultation measurements, *Icarus* **61**, 101–123, 1985.
- Kupo, I., Y. Mekler, and A. Eviatar, Detection of ionized sulphur in the jovian magnetosphere, *Astrophys. J.* **205**, L51–L54, 1976.
- Küppers, M. and K. Jockers, Fabry-Perot imaging of O III $\lambda = 5007$ Angstrom emission in the Io plasma torus, *Astrophys. J.* **441**, L101–L104, 1995.
- Küppers, M. and N. M. Schneider, The density of the Io plasma torus ribbon, *Geophys. Res. Lett.* **25**, 2757–2760, 1998.
- Küppers, M. and N. M. Schneider, Discovery of chlorine in the Io torus, *Geophys. Res. Lett.* **27**, 513–516, 2000.
- Kurth, W. S., A. Roux, S. J. Bolton, and C. F. Kennel, *Galileo* plasma wave observations in the Io plasma torus and near Io, *Science* **274**, 391–392, 1996.
- Lagg, A., N. Krupp, J. Woch, S. Livi, B. Wilken, and D. J. Williams, Determination of the neutral number density in the Io torus from *Galileo*-EPD measurements, *Geophys. Res. Lett.* **25**, 4039–4042, 1998.
- Landi, E., U. Feldman, and K. P. Dere, CHIANTI: An atomic database for emission lines. V. Comparison with an isothermal spectrum observed with SUMER, *Astrophys. J. Suppl. Ser.* **139**, 281–296, 2002.
- Lellouch, E., G. P. J. I. Moses, and N. M. Schneider, Jupiter i (Io), IAU Circ. 7803, 2002.
- Lichtenberg, G., *Massenbilanz und Energiehaushalt des Io-plasma-torus: Modell und Beobachtung*, Ph.D. thesis, University of Göttingen, Germany, 2000.
- Lichtenberg, G., N. Thomas, and T. Fouchet, Detection of S (IV) 10.51 μm emission from the Io plasma torus, *J. Geophys. Res.* **106**, 29 899, 2001.
- Linker, J. A., K. K. Khurana, M. G. Kivelson, and R. J. Walker, MHD simulations of Io's interaction with the plasma torus, *J. Geophys. Res.* **103**, 19 867–19 878, 1998.
- Matson, D. L., T. V. Johnson, and F. P. Fanale, Sodium D-line emission from Io: Sputtering and resonant scattering hypothesis, *Astrophys. J.* **192**, L43–L46, 1974.
- Mauk, B. H., S. A. Gary, M. Kane, E. P. Keath, S. M. Krimigis, and T. P. Armstrong, Hot plasma parameters of Jupiter's inner magnetosphere, *J. Geophys. Res.* **101**, 7685–7696, 1996.
- McGrath, M. and R. Johnson, Magnetospheric plasma sputtering of Io's atmosphere, *Icarus* **69**, 519, 1987.
- McNutt, R. L., J. W. Belcher, J. D. Sullivan, F. Bagenal, and H. S. Bridge, Departure from rigid co-rotation of plasma in Jupiter's dayside magnetosphere, *Nature* **280**, 803–, 1979.
- Melrose, D. B. and G. A. Dulk, On the elliptical polarization of Jupiter's decametric radio emission, *Astron. Astrophys.* **249**, 250–257, 1991.
- Mendillo, M., J. Baumgardner, B. Flynn, and W. J. Hughes, The extended sodium nebula of Jupiter, *Nature* **348**, 312–314, 1990.
- Meyer-Vernet, N., M. Moncuquet, and S. Hoang, Temperature inversion in the Io plasma torus, *Icarus* **116**, 202–213, 1995.
- Moncuquet, M., F. Bagenal, and N. Meyer-Vernet, Latitudinal structure of outer Io plasma torus, *J. Geophys. Res.* **107**, 24–1, 2002.
- Moreno, M. A. and D. D. Barbosa, Mass and energy balance of the cold Io torus, *J. Geophys. Res.* **91**, 8993–8997, 1986.
- Morgan, J. S., Temporal and spatial variations in the Io torus, *Icarus* **62**, 389–414, 1985.
- Moses, J. I., M. Y. Zolotov, and B. F. Jr, Photochemistry of a volcanically driven atmosphere on Io, *BAAS* **32**, 1057–1058, 2000.
- Neubauer, F. M., Nonlinear standing Alfvén wave current system at Io: Theory, *J. Geophys. Res.* **85**, 1171–1178, 1980.
- Olivero, R. J., F. Scherb, W. H. Smyth, M. E. Freed, R. C. Woodward, M. L. Marconi, K. D. Retherford, O. L. Lupie, and J. P. Morgenthaler, Sunlit Io atmospheric [O I] 6300 Å emission and the plasma torus, *J. Geophys. Res.* **106**, 26 183–26 194, 2001.
- Osterbrock, D. E., *Astrophysics of Gaseous Nebulae and Active Galactic Nuclei*, University Science Books, Mill Valley, California, 1989.
- Pearl, J., R. Hanel, V. Kunde, W. Maguire, K. Fox, S. Gupta, C. Ponnampereuma, and F. Raulin, Identification of gaseous SO₂ and new upper limits for other gases on Io, *Nature* **280**, 755–758, 1979.

- Piddington, J. H. and J. F. Drake, Electrodynamic effects of Jupiter's satellite Io, *Nature* **217**, 935, 1968.
- Pilcher, C. B. and J. S. Morgan, Detection of singly ionized oxygen around Jupiter, *Science* **205**, 297–298, 1979.
- Pilcher, C. B. and D. F. Strobel, Emissions from neutrals and ions in the jovian magnetosphere, in *The Satellites of Jupiter*, D. Morrison (ed), University of Arizona Press, pp. 807–845, 1982.
- Pilcher, C. B., W. H. Smyth, M. R. Combi, and J. H. Fertel, Io's sodium directional features: Evidence for a magnetospheric-wind-driven gas escape mechanism, *Astrophys. J.* **287**, 421–444, 1984.
- Pontius, D. H., Implications of variable mass loading in the Io torus: The jovian flywheel, *J. Geophys. Res.* **100**, 19531–19540, 1995.
- Pontius, D. H., The Io current wing, *J. Geophys. Res.* pp. 6–1, 2002.
- Pontius, D. H. and T. W. Hill, Departure from corotation of the Io plasma torus: Local plasma production, *Geophys. Res. Lett.* **9**, 1321–, 1982.
- Pontius, D. H. and T. W. Hill, Rotation driven plasma transport: The coupling of macroscopic motion and micro diffusion, *J. Geophys. Res.* **94**, 15041–15053, 1989.
- Pontius, D. H., T. W. Hill, and M. E. Rassbach, Steady state plasma transport in a corotation-dominated magnetosphere, *Geophys. Res. Lett.* **13**, 1097–1100, 1986.
- Pontius, D. H., R. A. Wolf, T. W. Hill, R. W. Spiro, Y. S. Yang, and W. H. Smyth, Velocity shear impoundment of the Io plasma torus, *J. Geophys. Res.* **103**, 19935–19946, 1998.
- Pospieszalska, M. K. and R. E. Johnson, Plasma heating of Io's atmosphere, *Geophys. Res. Lett.* **19**, 949–952, 1992.
- Rauer, H., T. Bonev, K. Jockers, and N. Thomas, Low-resolution spectra of the Io plasma torus 2 days after the *Ulysses* encounter, *Planet. Space Sci.* **41**, 1021–1028, 1993.
- Richardson, J. D. and R. L. McNutt, Observational constraints on interchange models at Jupiter, *Geophys. Res. Lett.* **14**, 64–67, 1987.
- Richardson, J. D. and G. L. Siscoe, Factors governing the ratio of inward to outward diffusing flux of satellite ions, *J. Geophys. Res.* **86**, 8485–8490, 1981.
- Richardson, J. D. and G. L. Siscoe, The problem of cooling the cold Io torus, *J. Geophys. Res.* **88**, 2001–2009, 1983.
- Roederer, J. G., *Dynamics of Geomagnetically Trapped Radiation*, Springer-Verlag, 1970.
- Roesler, F. L., J. L. Lowrance, P. Zucchini, D. Long, R. J. Oliverson, F. Scherb, J. Lattis, T. B. Williams, D. G. York, and E. B. Jenkins, Fabry-Perot/CCD observations of SIII and SII emissions from the Jupiter plasma torus, *Astrophys. J.* **259**, 900–907, 1982.
- Sagan, C., Sulphur flows on Io, *Nature* **280**, 750–753, 1979.
- Sandel, B. R. and A. J. Dessler, Dual periodicity of the jovian magnetosphere, *J. Geophys. Res.* **93**, 5487–5504, 1988.
- Saur, J., D. F. Strobel, F. M. Neubauer, and M. E. Summers, The ion mass loading rate at Io, *J. Geophys. Res.* **163**, 5487–5504, 2003.
- Scherb, F. and W. H. Smyth, Variability of (O I) 6300-Å emission near Io, *J. Geophys. Res.* **98**, 18729, 1993.
- Schneider, N. M. and J. T. Trauger, The structure of the Io torus, *Astrophys. J.* **450**, 450, 1995.
- Schneider, N. M., W. H. Smyth, and M. A. McGrath, Io's atmosphere and neutral clouds, in *Time-Variable Phenomena in the Jovian System*, pp. 75–99, NASA, SP-494, 1989.
- Schneider, N. M., J. T. Trauger, J. K. Wilson, D. I. Brown, R. W. Evans, and D. E. Shemansky, Molecular origin of Io's fast sodium, *Science* **253**, 1394–1397, 1991.
- Schneider, N. M., M. H. Taylor, F. J. Crary, and J. T. Trauger, On the nature of the λ_{III} brightness asymmetry in the Io torus, *J. Geophys. Res.* **102**, 19823–19834, 1997.
- Schreier, R., A. Eviatar, and V. M. Vasyliunas, A two-dimensional model of plasma transport and chemistry in the jovian magnetosphere, *J. Geophys. Res.* **103**, 19901–19914, 1998.
- Shemansky, D. E., Radiative cooling efficiencies and predicted spectra of species of the Io plasma torus, *Astrophys. J.* **236**, 1043–1054, 1980.
- Shemansky, D. E., Ratio of oxygen to sulfur in the Io plasma torus, *J. Geophys. Res.* **92**, 6141–6146, 1987.
- Shemansky, D. E., Energy branching in the Io plasma torus: The failure of neutral cloud theory, *J. Geophys. Res.* **93**, 1773–1784, 1988.
- Shemansky, D. E. and G. R. Smith, The *Voyager 1* EUV spectrum of the Io plasma torus, *J. Geophys. Res.* **86**, 9179–9192, 1981.
- Siscoe, G. L., On the equatorial confinement and velocity space distribution of satellite ions in Jupiter's magnetosphere, *J. Geophys. Res.* **82**, 1641–1645, 1977.
- Siscoe, G. L. and D. Summers, Centrifugally driven diffusion of iogenic plasma, *J. Geophys. Res.* **86**, 8471–8479, 1981.
- Siscoe, G. L., A. Eviatar, R. M. Thorne, J. D. Richardson, F. Bagenal, and J. D. Sullivan, Ring current impoundment of the Io plasma torus, *J. Geophys. Res.* **86**, 8480–8484, 1981.
- Sittler, E. C. and D. F. Strobel, Io plasma torus electrons: *Voyager 1*, *J. Geophys. Res.* **92**, 5741–5762, 1987.
- Skinner, T. E. and S. T. Durrance, Neutral oxygen and sulfur densities in the Io torus, *Astrophys. J.* **310**, 966–971, 1986.
- Smith, R. A. and D. F. Strobel, Energy partitioning in the Io plasma torus, *J. Geophys. Res.* **90**, 9469–9493, 1985.
- Smith, R. A., F. Bagenal, A. F. Cheng, and D. F. Strobel, On the energy crisis in the Io plasma torus, *Geophys. Res. Lett.* **15**, 545–548, 1988.
- Smyth, W. H., Neutral cloud distribution in the jovian system, *Adv. Space Res.* **12**, 8337–8346, 1992.
- Smyth, W. H. and M. R. Combi, A general model for Io's neutral gas clouds: II. Application to the sodium cloud, *Astrophys. J.* **328**, 888–918, 1988.
- Smyth, W. H. and M. R. Combi, The sodium zenocorona, *J. Geophys. Res.* **96**, 22711–22727, 1991.
- Smyth, W. H. and M. K. Marconi, Io's oxygen source: Determination from ground-based observations and implications for the plasma torus, *J. Geophys. Res.* **105**, 7783–7792, 2000.
- Smyth, W. H. and M. K. Marconi, Nature of iogenic plasma source in Jupiter's magnetosphere: I. Circumplanetary distribution, *J. Geophys. Res.* **in press**, 2003a.
- Smyth, W. H. and M. K. Marconi, Nature of iogenic plasma source in Jupiter's magnetosphere: II. Near-Io distribution, *J. Geophys. Res.* **submitted**, 2003b.
- Smyth, W. H. and M. L. Marconi, An explanation for the east-west asymmetry of the Io plasma torus, *J. Geophys. Res.* **103**, 9091–9100, 1998.
- Southwood, D. J. and M. G. Kivelson, Magnetospheric interchange instability, *J. Geophys. Res.* **92**, 109–116, 1987.
- Spitzer, L., *Physics of Fully Ionized Gases*, Interscience, 1962.
- Steffl, A., F. Bagenal, P. Delamere, and A. I. F. Stewart, *J. Geophys. Res.* **submitted**, 2003.
- Strobel, D. F., Energetics, luminosity and spectroscopy of Io's torus, in *Time-Variable Phenomena in the Jovian System*, M. J. S. Belton, R. A. West, and J. Rahe, eds, pp. 183–195, NASA SP-494, 1989.
- Strobel, D. F. and S. K. Atreya, Ionosphere, in *Physics of the Jovian Magnetosphere*, A. J. Dessler (ed.), Cambridge University Press, pp. 51–67, 1983.
- Su, Y.-J., R. Ergun, F. Bagenal, and P. Delamere, Io-related jovian auroral arcs: Modeling parallel electric fields, *J. Geophys. Res.* **108**, 1094, 2003.
- Summers, D. and G. L. Siscoe, Wave modes of the Io plasma torus, *Astrophys. J.* **295**, 678–684, 1985a.
- Summers, D. and G. L. Siscoe, Calculation of charge-state ratios for satellite tori, *Geophys. Res. Lett.* **12**, 753–756, 1985b.

- Summers, D. and G. L. Siscoe, A model of the Io plasma ribbon, *Icarus* **67**, 520–524, 1986.
- Summers, D., R. M. Thorne, and Y. Mei, Theory of centrifugally driven magnetospheric diffusion, *Astrophys. J.* **328**, 358–372, 1988.
- Summers, M. E., *Theoretical Studies of Io's Atmosphere*, Ph.D. thesis, California Institute of Technology, 1985.
- Summers, M. E. and D. F. Strobel, Photochemistry and vertical transport in Io's atmosphere and ionosphere, *Icarus* **120**, 290–316, 1996.
- Tayal, S. S., Collision strengths for electron collisional excitation of SII, *Astrophys. J. Suppl. Ser.* **111**, 459–466, 1997.
- Tayal, S. S. and G. P. Gupta, Collision strengths for electron collision excitation of fine-structure levels in SIII, *Astrophys. J.* **526**, 544–548, 1999.
- Taylor, M. H., N. M. Schneider, F. Bagenal, B. R. Sandel, D. E. Shemansky, P. L. Matheson, and D. T. Hall, A comparison of the *Voyager 1* ultraviolet spectrometer and plasma science measurements of the Io plasma torus, *J. Geophys. Res.* **100**, 19 541–19 550, 1995.
- Thomas, N., Optical observations of Io's neutral clouds and plasma torus, *Surv. Geophys.* **13**, 91–164, 1992.
- Thomas, N., Detection of OIII 5007 Å forbidden line emission from the Io plasma torus, *Astrophys. J.* **414**, L41–L44, 1993a.
- Thomas, N., The variability of the Io plasma torus, *J. Geophys. Res.* **98**, 18 737–18 750, 1993b.
- Thomas, N., High resolution spectra of Io's neutral potassium and oxygen clouds, *Astron. Astrophys.* **313**, 306–314, 1996.
- Thomas, N. and G. Lichtenberg, The latitudinal dependence of ion temperature in the Io plasma torus, *Geophys. Res. Lett.* **24**, 1175–1178, 1997.
- Thomas, N., D. E. Innes, and R. Lieu, Three-dimensional modelling of EUVE observations of the Io plasma torus, in *Astrophysics in the Extreme Ultraviolet*, p. 457, 1996.
- Thomas, N., G. Lichtenberg, and M. Scotto, High-resolution spectroscopy of the Io plasma torus during the *Galileo* mission, *J. Geophys. Res.* **106**, 26 277–26 292, 2001.
- Thorne, R. M., Microscopic plasma processes in the jovian magnetosphere, in *Physics of the Jovian Magnetosphere*, A. J. Dessler (ed.), Cambridge University Press, pp. 454–488, 1983.
- Thorne, R. M., T. P. Armstrong, S. Stone, D. J. Williams, R. W. McEntire, S. J. Bolton, D. A. Gurnett, and M. G. Kivelson, *Galileo* evidence for rapid interchange transport in the Io torus, *Geophys. Res. Lett.* **24**, 2131–2134, 1997.
- Tokar, R. L., D. A. Gurnett, and F. Bagenal, The proton concentration in the vicinity of Io plasma torus, *J. Geophys. Res.* **87**, 10 395–10 400, 1982.
- Trafton, L., Discovery of a potassium cloud near Io, *Nature* **258**, 690–692, 1975.
- Trafton, L., The jovian SII torus: Its longitudinal asymmetry, *Icarus* **42**, 111–124, 1980.
- Trafton, L., A survey of Io's potassium cloud, *Astrophys. J.* **247**, 1125–1140, 1981.
- Trafton, L., T. Parkinson, and W. Macy, The spatial extent of sodium emission around Io, *ApJ* **190**, L85+, 1974.
- Trauger, J. T., The jovian nebula: A post-*Voyager* perspective, *Science* **226**, 337–341, 1984.
- Vasyliunas, V. M., Low-energy electrons in the magnetosphere as observed by OGO-1 and OGO-3, in *Physics of the Magnetosphere*, p. 622, 1968.
- Vasyliunas, V. M., Plasma distribution and flow, in *Physics of the Jovian Magnetosphere*, A. J. Dessler (ed.), Cambridge University Press, pp. 395–453, 1983.
- Vasyliunas, V. M. and A. J. Dessler, The magnetic-anomaly model of the jovian magnetosphere: A post-*Voyager* assessment, *J. Geophys. Res.* **86**, 8435–8446, 1981.
- Volwerk, M., M. E. Brown, A. J. Dessler, and B. R. Sandel, Evidence for short cooling time in the Io plasma torus, *Geophys. Res. Lett.* **24**, 1147, 1997.
- Wang, K., R. M. Thorne, R. B. Horne, and W. S. Kurth, Cold torus whistlers: An indirect probe of the inner jovian plasmasphere, *J. Geophys. Res.* **103**, 14 987–14 994, 1998a.
- Wang, K., R. M. Thorne, R. B. Horne, and W. S. Kurth, Constraints on jovian plasma properties from a dispersion analysis of unducted whistlers in the warm Io torus, *J. Geophys. Res.* **103**, 14 979–14 986, 1998b.
- Warnecke, J., M. G. Kivelson, K. K. Khurana, D. E. Huddelston, and C. T. Russell, Ion cyclotron waves observed at *Galileo*'s Io encounter: Implications for neutral cloud distribution and plasma composition, *Geophys. Res. Lett.* **24**, 2139–2142, 1997.
- Williams, D., B. H. Mauk, R. E. McEntire, E. C. Roelof, T. P. Armstrong, B. Wilken, J. G. Roederer, S. M. Krimigis, T. A. Fritz, and L. J. Lanzerotti, Electron beams and ion composition measured at Io and its torus, *Science* **274**, 401–403, 1996.
- Williams, D. J., R. M. Thorne, and B. Mauk, Energetic electron beams and trapped electrons at Io, *J. Geophys. Res.* **104**, 14 739–14 754, 1999.
- Wilson, J. K., *Io's Fast Sodium Clouds and the Escape of Io's Ionosphere*, Ph.D. thesis, University of Colorado, Boulder, 1996.
- Wilson, J. K. and N. M. Schneider, Io's fast sodium: Implications for molecular and atomic atmospheric escape, *Icarus* **111**, 31–44, 1994.
- Wilson, J. K. and N. M. Schneider, Io's sodium directional features: Evidence for ionospheric escape, *BAAS* **28**, 1154, 1996.
- Wilson, J. K. and N. M. Schneider, Io's sodium directional feature: Evidence for ionospheric escape, *J. Geophys. Res.* **104**, 16 567–16 583, 1999.
- Wilson, J. K., M. Mendillo, J. Baumgardner, N. M. Schneider, J. T. Trauger, and B. Flynn, The dual sources of Io's sodium clouds, *Icarus* **in press**, 2002.
- Wong, M. C. and W. H. Smyth, Model calculations for Io's atmosphere at eastern and western elongations, *Icarus* **146**, 60–74, 2000.
- Woodward, R. C. J., *The Sulfur Emission and Periodicity of the Jupiter Plasma Torus in 1988*, Ph.D. thesis, University of Wisconsin, Madison, 1992.
- Woodward, R. C. J., F. Scherb, and F. L. Roesler, Variations in optical S+ emission from the Io plasma torus: Evidence for quasi-periodicity, *Astrophys. J.* **479**, 984, 1997.
- Woodward, R. C. J., R. J. Oliverson, F. Scherb, and F. L. Roesler, Synoptic imaging of the Io plasma torus in [S II] 6731 Å: Long-term variability, *BAAS*, 2000.
- Yang, Y. S., R. A. Wolf, R. W. Spiro, and A. J. Dessler, Numerical simulation of plasma transport driven by the Io torus, *Geophys. Res. Lett.* **19**, 957–960, 1992.
- Yang, Y. S., R. A. Wolf, R. W. Spiro, T. W. Hill, and A. J. Dessler, Numerical simulation of torus-driven plasma transport in the jovian magnetosphere, *J. Geophys. Res.* **99**, 8755–8770, 1994.
- Zarka, P., J. Queninnec, and F. J. Crary, Low-frequency limit of jovian radio emissions and implications on source locations and Io plasma wake, *Planet. Spa. Sci.* **49**, 1137–1149, 2001.

